HHS Public Access

Author manuscript

Mol Cell. Author manuscript; available in PMC 2022 May 20.

Published in final edited form as:

Mol Cell. 2021 May 20; 81(10): 2112–2122.e7. doi:10.1016/j.molcel.2021.03.004.

Convergence of mammalian RQC and C-end rule proteolytic pathways *via* alanine tailing

Anna Thrun[1], **Aitor Garzia**[2], **Yu Kigoshi-Tansho**[1], **Pratik R. Patil**[1], **Charles S. Umbaugh**[1], **Teresa Dallinger**[1], **Jia Liu**[1], **Sylvia Kreger**[1], **Annarita Patrizi**[3], **Gregory A. Cox**[4], **Thomas Tuschl**[2], **Claudio A.P. Joazeiro**[1,5,6,*]

[1]Center for Molecular Biology of Heidelberg University (ZMBH), DKFZ-ZMBH Alliance, 69120 Heidelberg, Germany

[2]Laboratory of RNA Molecular Biology, The Rockefeller University, New York, NY 10065, USA

[3]Schaller Research Group Leader at the German Cancer Research Center, DKFZ-ZMBH Alliance, 69120 Heidelberg, Germany.

[4]The Jackson Laboratory, Bar Harbor, ME 04609, USA

[5]Department of Molecular Medicine, Scripps Research, Jupiter, FL 33458, USA

[6]Lead Contact

SUMMARY

Incompletely-synthesized nascent-chains obstructing large ribosomal subunits are targeted for degradation by Ribosome-associated Quality Control (RQC). In bacterial RQC, RqcH marks the nascent-chains with C-terminal alanine (Ala) tails that are directly recognized by proteasome-like proteases, whereas in eukaryotes, RqcH orthologs (Rqc2/NEMF) assist the Ltn1/Listerin E3 ligase in nascent-chain ubiquitylation. Here we study RQC-mediated proteolytic targeting of ribosome stalling products in mammalian cells. We show that mammalian NEMF has an additional, Listerin-independent proteolytic role which, as in bacteria, is mediated by tRNA-Ala binding and Ala tailing. However, in mammalian cells Ala tails signal proteolysis indirectly, through a pathway that recognizes C-terminal degrons—we identify the CRL2^{KLHDC10} E3 ligase complex and the novel C-end rule E3, Pirh2/Rchy1, as *bona-fide* RQC pathway components that directly bind to Ala-tailed ribosome stalling products and target them for degradation. As Listerin mutation causes

*Correspondence: c.joazeiro@zmbh.uni-heidelberg.de.

AUTHOR CONTRIBUTIONS

A. T. generated all stable RPE1 cell lines, designed, performed and analyzed most experiments, and generated the figures. A. G. performed and analyzed PAR-CLIP experiments. Y. K.-T. generated the HeLa CRISPR NKO cell line and performed initial experiments to set up this mammalian cell model to study RQC. C. S. U. generated HeLa LKO, HeLa LNKO and RPE1 LKO cell lines. P. P. performed *in vitro* binding assays. T. D. assisted with protein purifications and *in vitro* ubiquitylation assays. J. L. set up FACS analyses to monitor GFP reporter stability. S. K. provided technical and managerial assistance. G. C. provided variant GFP fusion constructs. A. P. provided laboratory space and resources. C. A. P. J. designed studies, conceived and supervised the project and wrote the manuscript with contributions from A. T. All authors commented on the manuscript.

DECLARATION OF INTERESTS

The authors declare no competing interests.

neurodegeneration in mice, functionally-redundant E3s may likewise be implicated in molecular mechanisms of neurodegeneration.

Graphical Abstract

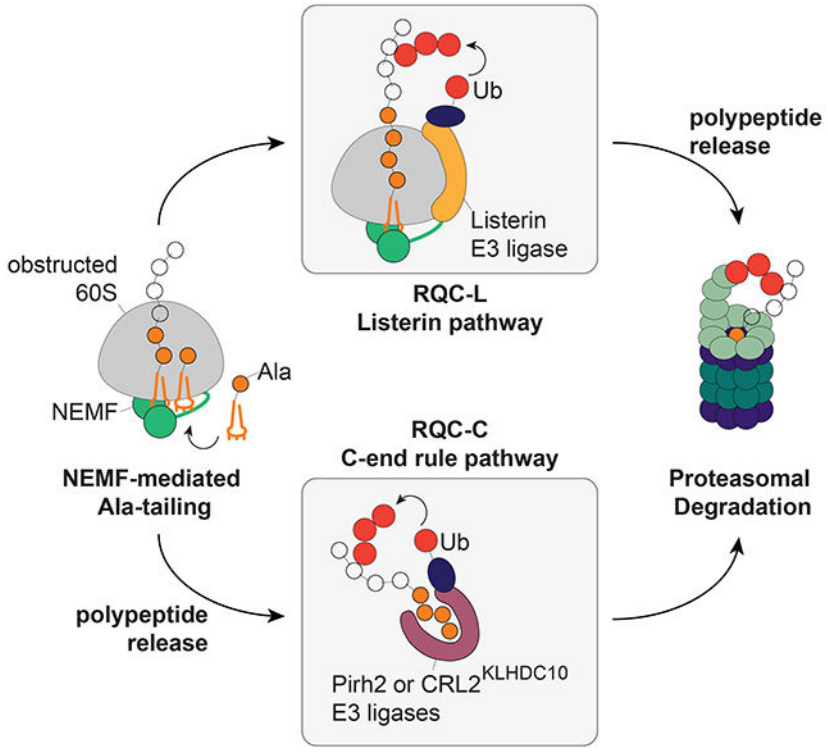

eTOC blurb

NEMF acts in Ribosome-associated Quality Control (RQC), which targets nascent-chains obstructing large ribosomal subunits for proteolysis. The functions of NEMF homologs in bacteria and yeast are mediated by nascent-chain modification with C-terminal tails. Whether such modification also occurs in mammals has remained unknown. Thrun et al. show that human NEMF recruits tRNA-Ala to modify nascent-chains with alanine tails, which are targeted by E3 ligases for ubiquitylation.

INTRODUCTION

A hallmark of human neurodegenerative disease is the accumulation and aggregation of aberrant proteins in affected neurons (Ross and Poirier, 2004, Luh and Bertolotti, 2020). It is thus reasonable to expect that the understanding of protein quality control processes will contribute to the elucidation of molecular mechanisms underlying these diseases and the identification of new therapeutic opportunities. However, while ubiquitin-mediated proteasomal degradation is part of the front line of defense against aberrant protein production in eukaryotic cells (Joazeiro, 2019, Pohl and Dikic, 2019, Finley, 2011), the identity and mechanisms of E3 ligases involved in protein quality control is only beginning to be uncovered (Defenouillere and Fromont-Racine, 2017, Joazeiro, 2019).

A principle of E3 ligase function in protein surveillance that has already emerged is that these enzymes can act in a more specialized manner than previously thought (Defenouillere and Fromont-Racine, 2017, Joazeiro, 2019). For example, we had originally found that aberrant proteins generated by the stalling of ribosomes during translation are targeted by the 60S ribosomal subunit-associated yeast E3 ligase Ltn1 (Bengtson and Joazeiro, 2010) (Listerin in mammals) in a process now known as Ribosome-associated Quality Control (RQC). Consistent with having an important role in protein quality control, Listerin mutation causes neurodegeneration in mice (Chu et al., 2009).

In the RQC pathway, ribosomes stalled during translation are first sensed and recycled by factors that promote subunit dissociation but leave behind a nascent-chain still conjugated to tRNA obstructing the large (60S) subunit (Shoemaker et al., 2010, Pisareva et al., 2011, Shao et al., 2013). In eukaryotes, Rqc2/NEMF senses the obstruction and recruits Ltn1 to an "RQC complex" that targets the nascent-chain for disposal (Lyumkis et al., 2014, Shen et al., 2015, Shao et al., 2015, Defenouillere et al., 2013, Brandman et al., 2012, Bengtson and Joazeiro, 2010). In addition, yeast Rqc2 recruits tRNA-Ala and -Thr to elongate the nascent-chain with C-terminal Ala and Thr tracts (CAT tails) (Shen et al., 2015; Osuna et al., 2017), which further assists Ltn1 by exposing Lys residues buried in the ribosomal exit tunnel for ubiquitylation (Kostova et al., 2017). We have recently found that RQC is also present in bacteria, mediated by the Rqc2/NEMF ortholog, RqcH (Lytvynenko et al., 2019). Notably, after sensing obstruction of the large (50S) subunit, bacterial RqcH elongates the nascent-chains with Ala tails, which are directly recognized by proteasome-like proteases like ClpXP for degradation (Lytvynenko et al., 2019). Whether mammalian NEMF also modifies nascent-chains with C-terminal tails, as well as the composition of such tails and their functions, has remained unknown.

RESULTS

NEMF promotes degradation of ribosome stalling products independently of Listerin

To study RQC-mediated protein degradation in mammalian cells we utilized a bicistronic reporter construct (Yen et al., 2008) encoding the DsRed reference protein followed by an internal ribosomal entry site (IRES) driving translation of either GFP or GFP lacking in-frame stop codons, referred to as GFP non-stop (NS) (Figure 1A). In NS transcripts, ribosomes stall upon translation of poly(A) sequences, triggering RQC activation and NS protein degradation (Bengtson and Joazeiro, 2010, Garzia et al., 2017a, Juszkiewicz and Hegde, 2017, Chandrasekaran et al., 2019). Because both GFP and DsRed are translated from the same mRNA, RQC-mediated effects in GFP NS stability can be monitored through changes in the GFP/DsRed ratio. As previously reported in various model systems (e.g., (Saito et al., 2013, Bengtson and Joazeiro, 2010, Lytvynenko et al., 2019)), expression of GFP NS was reduced compared to GFP ("WT" in Figure 1B; Figure S1A) and was increased upon inhibition of the proteasome (Figure S1A). GFP NS stability was also increased by depletion of either Listerin or NEMF (Figure 1B). Similar findings were made using stable gene knockout in HeLa cells (Figures 1B and S1B) and transient siRNA-mediated knockdown in RPE1 cells (Figures S1C,D), indicating that the effects were not depletion approach- or cell line-specific. Importantly, we observed that the simultaneous

depletion of both Listerin and NEMF resulted in a greater extent of NS reporter stabilization compared to depletion of either factor alone (Figures 1B and S1C). That NEMF was not essential for GFP NS degradation was not unexpected, as Listerin is able to bind alone to the 60S subunit, albeit less stably, in both mammalian and yeast systems (Shao and Hegde, 2014, Lyumkis et al., 2014, Defenouillere et al., 2013). However, NEMF's ability to promote GFP NS degradation in Listerin's absence was surprising, given that NEMF was previously thought to act in nascent-chain proteolysis primarily by supporting Listerin's function. Providing further evidence of a Listerin-independent proteolytic role of NEMF, GFP NS-associated ubiquitin signal was also strongly reduced in cells in which both *LTN1* and *NEMF* had been knocked out, in comparison to cells depleted for either RQC component alone, even though more GFP NS was immunoprecipitated (IP'ed) from the double-knockout (LNKO) cells (Figure 1C). These results suggest that NEMF can promote Listerin-independent ubiquitylation and degradation of proteins produced by ribosome stalling in mammalian cells.

C-terminal Ala tails act as degrons for the ubiquitin-proteasome system

NEMF orthologs in yeast and bacteria have the intrinsic ability to elongate nascent-chains obstructing the large ribosomal subunit at the C-terminus with either Ala and Thr, or Ala-only tracts, respectively (Shen et al., 2015, Lytvynenko et al., 2019). Of note, such C-terminal tails mark nascent-chains for degradation in bacteria (Lytvynenko et al., 2019) and may have some proteolytic function in yeast as well (Sitron and Brandman, 2019). We thus set out to investigate whether NEMF likewise makes C-terminal tails, and whether that underlies the Listerin-independent non-stop protein degradation promoted by NEMF.

C-terminal extension of nascent-chains by RqcH and Rqc2 is mediated by their recruitment of tRNA-Ala, or tRNA-Ala and -Thr, respectively (Shen et al., 2015, Lytvynenko et al., 2019). We thus set out to identify tRNAs that bind to NEMF using an unbiased and quantitative approach. Cells expressing FLAG-tagged NEMF were subjected to 4-thiouridine photoactivatable ribonucleoside-enhanced cross-linking followed by FLAG IP (PAR-CLIP) (Garzia et al., 2017b, Gogakos et al., 2017). RNA crosslinked to NEMF was isolated, deep-sequenced, and analyzed for T-to-C conversions, which are the readout for protein-RNA crosslinking sites (Figures 2A,B and S2). NEMF predominantly cross-linked to tRNAs, followed by 28S rRNA (Figures S2A and S2E). Among all tRNAs, tRNA-Ala(AGC) with the common adenine to inosine (A-to-I) modification at position 33 in the anticodon (i.e., IGC; Figure S2C-D) was by far the most highly enriched in crosslinked reads relative to the respective cellular abundance, while tRNA-Thr, which is part of CAT-tail synthesis in yeast, was not enriched (Figures 2A and S2B). Further highlighting the specificity of these findings, tRNA-Lys was also not enriched in the NEMF analyses while it was the predominant tRNA species crosslinked to the RNA-binding protein ZNF598 (Garzia et al., 2017a). Notably, the NEMF crosslinking positions in tRNA-Ala were mapped to the immediate vicinity of the anticodon (Figure 2B), in agreement with cryo-EM structures of yeast and bacterial NEMF orthologs bound to the obstructed large subunit suggesting how NEMF recruits the tRNA for C-terminal tailing (Shen et al., 2015, Filbeck et al., 2021, Crowe-McAuliffe et al., 2021). In contrast, all other tRNAs, such as tRNA-Lys UUU, were mostly crosslinked to NEMF *via* the D-loop (Figure 2B). This distinct pattern might result

from (inefficient) crosslinking of, e.g., tRNAs already present in the ribosomal P-site during initial NEMF-60S binding, or tRNAs nonspecifically bound to NEMF.

The above results, together with similar findings for *B. subtilis* RqcH (Lytvynenko et al., 2019), supported a model in which NEMF binds tRNA-Ala to make C-terminal Ala tails. To begin testing whether Ala tailing might account for NEMF's Listerin-independent proteolytic function, GFP was fused to C-terminal homopolymeric Ala tracts of different lengths followed by a stop codon, and analyzed by flow cytometry. The results show that a C-terminal polyAla tract indeed destabilized GFP, with four or more Ala residues being required for maximal effect of homopolymeric sequences (Figure 2C). Extending an Ala_5 sequence with a single Thr led to complete loss of destabilizing activity, suggesting that polyAla-mediated protein degradation requires sensing of both a C-terminal Ala and its α-COOH group, and implies that polyAla tracts internal to proteins would lack a similar destabilizing property. We also conclude that the requirement for at least four C-terminal Ala for destabilization was not due to steric clashes with GFP preventing accessibility to a single Ala at the end of shorter tails, since Thr_2Ala_2 had no destabilizing effect (Figure 2C). Finally, we tested the effect of placing Lys residues immediately N-terminal to the Ala tail on degron function, as translation of the poly(A) sequence in a non-stop mRNA appends a Lys tract to the non-stop protein, which would precede the NEMF-mediated Ala modification. The results show that, while a hard-coded Lys_4 sequence was not destabilizing, Lys_4Ala_4 was (Figure 2C). Thus, C-terminal Ala tails can act as degrons and are sufficient for this activity.

To investigate the general pathway underlying GFP-Ala_6 degradation, we tested the effect of pharmacological inhibition of the proteasome, and found that this resulted in a greater than 10-fold increase in the reporter levels (Figure 2D). In addition, pull down of GFP-Ala_6 followed by anti-ubiquitin (or anti-GFP) immunoblot revealed a ladder of ~8-kDa incrementally larger bands above the unmodified reporter band, indicating that GFP-Ala_6 was ubiquitylated (Figure 2E). Thus, reporter destabilization caused by fusion to an Ala tail was mediated by the ubiquitin-proteasome system.

Ala tails are recognized by the E3 ligases Pirh2 and $CRL2^{KLHDC10}$

We next set out to identify the Ala tail-targeting E3 ligase(s). Immunoprecipitation followed by mass spectrometry (IP/MS) uncovered as the top hits specifically co-IP'ed with GFP-Ala_6: the E3 ligase Pirh2 (p53-induced RING-H2 protein; also known as Rchy1, for RING finger and CHY zinc finger domain-containing protein 1); all subunits of the cullin-RING ligase (CRL) complex $CRL2^{KLHDC10}$ (namely, the substrate-binding receptor KLHDC10, the adapters Elongins B and C, and the scaffolding protein Cullin-2; the small RING domain subunit Rbx1 was also identified, but was not among the top hits); the CRL-activating ubiquitin-like modifier Nedd8; and the E2 enzyme UBE2D3 (Tables S1 and S2, Figure 3A). Confirming the IP/MS results, the unstable GFP-Ala_6 and GFP-Ala_4 reporters, but not the stable GFP or GFP-Thr_2Ala_2 reporters, co-IP'ed with FLAG-tagged Pirh2 and KLHDC10 (Figures 3B-C; see also Figure 2C). The presence of Leu, Phe or Val at the C-terminus of GFP-Ala_5 impaired the co-IP with Pirh2 and KLHDC10 (Figure S3A) suggesting that these C-end E3 ligases do not recognize hydrophobicity in general. Finally, we provide evidence

that the E3 ligase-Ala tail interactions were direct, as recombinant Pirh2 and KLHDC10 were competent to both pull down (Figure S3B) and ubiquitylate (Figure S3C) GFP-Ala_6 *in vitro*, in reactions with all components purified from bacteria.

The finding of KLHDC10 as an Ala tail-interacting E3 ligase was encouraging, as KLHDC10 and the closely related CRL2 substrate-binding receptors KLHDC2 and KLHDC3 had been shown to recognize specific C-terminal degrons in the context of the recently-discovered C-end rule pathway (KLHDC10 substrates were enriched for -TrpGly, -ProGly and -AlaGly) (Koren et al., 2018, Rusnac et al., 2018, Lin et al., 2018). Underscoring the specificity of the KLHDC10-Ala tail interaction, KLHDC2 failed to co-IP with GFP-Ala_6 (Figure 3D; indeed, although KLHDC2 has been found to bind to degrons with a C-terminal Ala, Gly was required at the penultimate position; (Lin et al., 2018)). On the other hand, Pirh2 was not previously known to target C-terminal degrons and has been best characterized as an E3 ligase that ubiquitylates p53 in response to DNA damage (Leng et al., 2003).

To validate Pirh2 and $CRL2^{KLHDC10}$ as Ala-tail-targeting E3 ligases, we first examined whether GFP-Ala_6 ubiquitylation depended on them. The anti-GFP immunoblot in Figure 3B had already revealed that overexpression of Pirh2, but not the E3 ligase-defective mutant Pirh2 M176E (Sheng et al., 2008), sufficed to increase ubiquitylation of GFP-Ala_6. Conversely, using a loss-of-function approach we found that GFP-Ala_6 was not ubiquitylated when expressed in cells depleted for both Pirh2 and KLHDC10 (Figures 3E and S3D; we note that GFP-Ala_6 had different patterns of ubiquitylation remaining in cells in which the E3s had been knocked down individually—GFP-Ala_6 was found associated with higher molecular weight ubiquitylated species upon Pirh2 knockdown, and with a lower molecular weight ubiquitin ladder upon KLHDC10 knockdown. While the nature of such modifications has not been examined further, we presume they could represent, e.g., polyubiquitylation versus multiple monoubiquitylation, respectively).

Correlating with the above ubiquitylation results, knocking down Pirh2 or KLHDC10 individually was not sufficient to stabilize GFP-Ala_6 (Figures 3F and S4A-C), whereas knocking down both E3s simultaneously led to greatly increased GFP-Ala6 levels; in contrast, depletion of KLHDC2 and KLHDC3, alone or together with Pirh2, failed to stabilize GFP-Ala_6 (Figures S4C-E). Finally, MLN4924, a compound that inhibits CRLs in general (Soucy et al., 2009), did not stabilize GFP-Ala_6 on its own, but did have a synergistic effect on GFP-Ala_6 stability in combination with Pirh2 depletion (Figure 3F). Together, these results suggest that Pirh2 and $CRL2^{KLHDC10}$ act redundantly in promoting degradation of GFP-Ala_6.

We next began testing whether Pirh2 and $CRL2^{KLHDC10}$ were able to target Ala-containing C-terminal sequences found in the human proteome. GFP fusion to the C-terminal 23 residues of the cytosolic protein TRAPPC11, which ends in 3 Ala (-MDDTSI**AAA**), sufficed to cause strong reduction in GFP levels (Figure S4F; this contrasts with GFP-Ala_3, which was only partially unstable in our assay compared to GFP-Ala_6 (Figure 2C)). Furthermore, expression of the fusion protein was restored to parental GFP levels upon depletion of the E3s, with KLHDC10 having a stronger effect in comparison to Pirh2 when

depleted alone (Figure S4F). These results suggest that, in addition to targeting homopolymeric Ala tails, Pirh2 and CRL2^{KLHDC10} may use the same binding mode to target native proteins harboring Ala-rich C-degrons.

Pirh2 and KLHDC10 function in RQC

We next sought evidence that Pirh2 and CRL2^{KLHDC10} function in the context of the RQC pathway. The data presented above support a model in which the products of ribosome stalling that become Ala-tailed by NEMF would be targeted for ubiquitylation and degradation by the Pirh2 and CRL2^{KLHDC10} E3 ligases. To test the model, we first asked whether FLAG-tagged E3 ligases could physically interact with the GFP NS stalling reporter, by performing GFP IP followed by anti-FLAG immunoblot. The results show that, as predicted, the Ala tail-binding proteins Pirh2 and KLHDC10 co-IP'ed with the ribosome stalling reporter, but not with the parental reporter, and that binding was NEMF-dependent (Figures 4A and S5A,B).

C-terminal tailing by Rqc2 and RqcH requires residues that are highly conserved among NEMF orthologs, equivalent to NEMF's Asp96 and Arg97 (Shen et al., 2015, Lytvynenko et al., 2019, Yonashiro et al., 2016, Choe et al., 2016, Defenouillere et al., 2016, Filbeck et al., 2021). To pursue further evidence that the above NEMF-dependent interaction was due to an Ala tail requirement, NEMF- and Listerin-deficient cells were reconstituted with NEMF wild type (WT) or D96A R97A ("DR") mutant and used for testing the binding of KLHDC10 to GFP NS. The results show that, while both NEMF proteins were expressed at comparable levels, NEMF WT but not the predicted Ala-tailing-deficient mutant enabled the co-IP of KLHDC10 with GFP NS (Figure 4B), supporting the model that the interaction is mediated by Ala tails added to GFP NS by NEMF.

We also verified whether Pirh2 and KLHDC10 were required for GFP NS ubiquitylation. As expected, the results show that GFP NS ubiquitylation was decreased when Listerin was simultaneously depleted with either Pirh2 or KLHDC10 (Figures S5C-E), and more markedly so in cells deficient for all three E3 ligases (Figures 4C, lane 7, and S5C-E), under which conditions the weak residual GFP NS-associated ubiquitin signal was comparable to that observed upon simultaneous depletion of Listerin and NEMF (Figure 4C, lane 6; see also Figure 1C). Moreover, also supporting the model that the function of Pirh2 or KLHDC10 in RQC is NEMF-dependent, GFP-NS ubiquitylation did not appear to be further reduced by depletion of these E3 ligases in cells lacking Listerin and NEMF (Figure 4C, compare lanes 6 and 8) or by loss of NEMF function in cells depleted for Listerin, Pirh2 and KLHDC10 (Figure 4C, compare lanes 7 and 8). In correlation with these ubiquitylation data, flow cytometry analysis revealed that levels of GFP NS in Listerin-null cells were increased upon depletion of Pirh2 and KLHDC10, and that GFP-NS stabilization in response to C-end E3 ligase knockdown required NEMF's presence (Figure 4D). These results support the model that the activities of Pirh2 and CRL2^{KLHDC10} underlie the Listerin-independent, NEMF-mediated ubiquitylation and degradation of ribosome stalling products.

Finally, we tested the model prediction that depletion of Pirh2 and KLHDC10 should lead to accumulation of Ala tail-modified stalling products. Strikingly, a slower-migrating GFP NS band became evident upon knock down of both E3s and the appearance of this band was

strictly dependent on NEMF (Figures 4E and S6A-D). These results are consistent with previous findings in yeast RQC showing that CAT tailing forms slower-migrating stalling reporter species (e.g., (Shen et al., 2015, Yonashiro et al., 2016, Choe et al., 2016, Defenouillere et al., 2016)) and provide physical evidence for a modification correlating with Ala tailing.

DISCUSSION

NEMF orthologs are found in all domains of life (Burroughs and Aravind, 2014). In yeast, Rqc2 has been known to modify nascent-chains obstructing large ribosomal subunits with Ala and Thr tails (Shen et al., 2015; Osuna et al., 2017), which facilitate ubiquitylation by the 60S-associated Ltn1/Listerin E3 ligase (Kostova et al., 2017) (Bengtson and Joazeiro, 2010) and may also have functions off the ribosome (Sitron and Brandman, 2019, Yonashiro et al., 2016, Choe et al., 2016, Defenouillere et al., 2016), whereas the bacterial ortholog (RqcH) marks nascent-chains with Ala tails that act as degrons (Lytvynenko et al., 2019). Whether C-terminal tailing also occurs in mammals, as well as the function of C-terminal tailing in mammalian RQC, had remained unknown. Our results show that NEMF-dependent polypeptide elongation indeed occurs in human cells, that NEMF generates Ala tails, and that Ala tails act as a novel signal for substrate targeting in the ubiquitin-proteasome system (UPS)—thus mediating aberrant nascent-chain ubiquitylation and degradation independently of Listerin. In addition, the work uncovers the E3 ligases responsible: Pirh2/Rchy1 and $CRL2^{KLHDC10}$ act as *bona fide* components of RQC that recognize the Ala-tailed substrates, broadening the perspective of RQC in mammals.

Pirh2/Rchy1 and $CRL2^{KLHDC10}$ function as C-end rule E3 ligases, which target proteins that harbor C-terminal degrons for ubiquitylation. The C-end rule was discovered by previous work identifying a variety of C-terminal destabilizing motifs along with the E3 ligases responsible for the destabilizing effect (Koren et al., 2018, Lin et al., 2018). In addition to being naturally present in full-length human proteins, likely playing a role in constitutive turnover, C-degrons were also suggested to be generated *de novo*, as a consequence of truncation or proteolytic cleavage ((Varshavsky, 2019) and Figure S4F). Our results now indicate that a protein modification—namely, Ala tailing—also generates C-end rule substrates, and uncovers a physiological role for the C-end rule in protein quality control.

A model for NEMF-mediated and Listerin-independent targeting of RQC substrates for degradation

Our results support a model in which, following the sensing of 60S subunit obstruction, NEMF extends the nascent-chains at the C-terminus with Ala tails (Figure 5). Nascent-chains can then have at least two alternative fates: in the canonical RQC pathway (RQC-L, for Listerin), NEMF recruits Listerin to ubiquitylate nascent-chains while they are still 60S-associated. In this pathway, NEMF's C-terminal tailing activity can assist Listerin by exposing Lys residues buried in the ribosomal exit tunnel for ubiquitylation (Kostova et al., 2017). Ubiquitylated nascent-chains are then released and degraded by the proteasome. In the alternative pathway described here, NEMF has a Listerin-independent degradation function. The release of nascent-chains from the 60S subunit exposes the Ala tail

modification, enabling its recognition by the Pirh2 or $CRL2^{KLHDC10}$ E3 ligases (hence RQC-C, for C-end rule), which mark the aberrant polypeptides with ubiquitin for degradation.

Our finding of at least two E3 ligases that can act redundantly with Listerin in RQC, along with the conservation of C-terminal tailing as a proteolytic tagging mechanism in RQC from bacteria to mammals (this work; (Lytvynenko et al., 2019, Sitron and Brandman, 2019)) and the neurodegenerative phenotype of mice and humans with RQC mutations (Chu et al., 2009, Martin et al., 2020), implies that products of failed translation pose a critical problem to cellular fitness. Along these lines, one direction of future work will be aimed at investigating the role of Pirh2 and $CRL2^{KLHDC10}$ in neurodegeneration caused by the Listerin mutation (Chu et al., 2009). Our results raise the possibility that Listerin-mutant mice manifest a phenotype that is attenuated by the action of these E3 ligases, although an alternative scenario is, conceivably, that RQC-C does not play any protective role against the neurodegenerative phenotype because it is not normally functional in the affected cells.

Below we discuss additional implications of the model and directions for future research.

Relative contributions of RQC-C *versus* RQC-L

Our findings raise the question, to what extent is RQC-C active when Listerin is present? That RQC-C takes place in WT cells is revealed by the accumulation of Ala-tailed NS reporter upon depletion of Pirh2 and KLHDC10 (Figures 4E and S6A,C). Consistent with this observation, the NS reporter was also co-IP'ed from WT cells with KLHDC10 (Figure S5A). However, Pirh2 and KLHDC10 depletion only led to little increase of NS reporter levels in WT cells (Figure 4D) suggesting that RQC-L is prevalent, at least for the experimental system utilized in this work. Future investigation will address the relative contributions of RQC-L- vs. RQC-C-mediated degradation of non-stop proteins in alternative contexts, as the contribution of RQC-C may become more prominent under yet unidentified conditions in which Listerin expression or activity is limiting—perhaps in some cell types, under certain stresses, or with a subset of substrates, such as those lacking Lys residues readily accessible for ubiquitylation by Listerin (which may be the case for a majority of substrates stalled on the ER translocon; see (von der Malsburg et al., 2015, Joazeiro, 2019)).

Nascent-chain release mechanism

Ala-tailed nascent-chains must be released from the large ribosomal subunits to be recognized by Pirh2 and KLHDC10. The best characterized mechanism for nascent-chain release in RQC involves tRNA cleavage by the ANKZF1 endonuclease. However, ANKZF1 cleavage leaves 3 nucleotides still linked to the polypeptides (Verma et al., 2018, Yip et al., 2019) whereas our results suggest that such polypeptides with a blocked C-terminus would not serve as substrates for Pirh2 and KLHDC10. Consistently, biochemical studies show that the ANKZF1 mechanism may preferentially take place after nascent-chains are ubiquitylated by Listerin (Kuroha et al., 2018) while, in the absence of Listerin, nascent-chains were found to be released free of nucleotides by the canonical peptidyl-tRNA hydrolase Ptrh1 (Kuroha et al., 2018). The existence of alternative release mechanisms is

thus in agreement with the RQC-L and RQC-C pathways proposed here, with the 3-nucleotide remnant generated by ANKZF1 perhaps serving as a mark to prevent unnecessary engagement of the C-end rule E3 ligases with substrates that have already been ubiquitylated by Listerin.

Evolutionary conservation of Ala tails as a proteolytic signal

This work reveals the deep evolutionary conservation of Ala tails as a proteolytic signal—from bacteria, where they are directly recognized by proteasome-like proteases like ClpXP, to mammalian cells, where they are recognized by specific C-end rule E3 ligases for ubiquitin tagging.

Notably, in *S. cerevisiae*, Rqc2 modifies nascent-chains with both Ala and Thr residues. The above evolutionary distribution of Ala tails suggests that Thr was likely incorporated secondarily as a major C-terminal tail component during yeast evolution and raises the question of what the function of Thr in such CAT tails is. Notably, the Ala and Thr combination has a synergistic effect in increasing the amyloid-aggregation propensity of C-terminal tails (Yonashiro et al., 2016, Choe et al., 2016, Defenouillere et al., 2016) raising the possibility that CAT tails in yeast may have evolved primarily to promote protein aggregation in case Ltn1 fails, perhaps to sequester and/or enable elimination of the aberrant proteins *via* aggrephagy. It has also been suggested that CAT tails may mediate Ltn1-independent proteolysis (Sitron and Brandman, 2019), but in this case the random incorporation of Thr residues during tail synthesis generates heterogeneous sequences in nature (Shen et al., 2015) that would render CAT tails less efficient as degrons in imparting recognition by specialized E3 ligases. Accordingly, only a small subset of engineered CAT tail sequences appeared to have an Ltn1-independent proteolytic function (Sitron and Brandman, 2019).

How certain CAT tail sequences may confer instability to appended proteins remains to be determined, although the mechanism is presumably distinct from the one reported here. The C-end rule pathway has not been reported in *S. cerevisiae*, and this organism lacks homologs of Pirh2 and of CRL2 subunits (Cul2, Elongins B/C and substrate adaptors). Conversely, the Hul5 E3 ligase was required for degradation of some CAT tails in yeast (Sitron and Brandman, 2019), but we have not observed a requirement for the Hul5 ortholog in Ala-tailed reporter degradation in mammalian cells (Figures S7A,B). We note that Hul5 is a proteasome-associated E3 ligase that has been implicated in the degradation of misfolded proteins in general (Fang et al., 2011, Finley, 2011). It is thus conceivable that destabilizing CAT tails may act directly at the level of the proteasome. An exciting concept is that CAT tails (and possibly Ala tails) may initiate protein unfolding at the proteasome thus facilitating degradation, as described for certain C-terminal sequences (Prakash et al., 2004, Tomita and Matouschek, 2019).

Limitations

Although the precise identity and length of the C-terminal tails made by NEMF remains to be determined by direct analysis of modified proteins, our NEMF-RNA crosslinking studies support the model that the tails consist of Ala —tRNA-Ala was strongly enriched in

comparison to other tRNAs (Figure 2A) and selective tRNA binding by NEMF orthologs was highly predictive of the composition of tails formed in the yeast and bacterial systems (Shen et al., 2015, Lytvynenko et al., 2019). The PAR-CLIP results are also consistent with the finding that the bacterial NEMF ortholog generates Ala tails (Lytvynenko et al., 2019). Finally, we show that Ala tails underlie the biological process we set out to investigate—we have tested the model that Ala tails mediate the Listerin-independent proteolytic function of NEMF and found that hard-coded C-terminal Ala tracts sufficed to destabilize a reporter protein, while the addition of a single Thr at the very C-terminus of an Ala tract abolished its destabilizing activity; moreover, we have identified two E3 ligases from crude cell extracts based solely on their ability to bind a GFP-Ala_6 fusion protein and, returning to the RQC analyses, we have demonstrated that those E3 ligases indeed targeted substrates of the pathway and did so in a NEMF-dependent manner.

STAR METHODS

RESOURCE AVAILABILITY

Lead Contact—Further information and requests for resources and reagents should be directed to and will be fulfilled by the Lead Contact, Claudio A. P. Joazeiro (c.joazeiro@zmbh.uni-heidelberg.de).

Materials Availability—All unique/stable reagents generated in this study are available from the Lead Contact.

Data and Code Availability—The NCBI SRA accession number for the NEMF PAR-CLIP sequencing data reported in this paper is PRJNA641646. All raw files of immunoblots were submitted to Mendeley data accessible under the following link: http://dx.doi.org/10.17632/vytk5p9wn6.1

EXPERIMENTAL MODEL AND SUBJECT DETAILS

Cell lines—HeLa and RPE1 cells were cultured at 37°C and 5% CO_2 in DMEM (Gibco) and DMEM/F12 (Gibco), respectively, supplemented with 10% v/v FBS (Gibco) and 2 mM L-Glutamine (Gibco). RPE1 cells stably expressing DsRed-IRES-GFP, -GFP-Ala_6, or -GFP NS were maintained using 0.2 mg/ml G418. Flp-In T-REx 293 cells (Thermo Fisher Scientific, R78007) were grown in high glucose DMEM (Thermo Fisher Scientific) supplemented with 10% v/v FBS, 100 U/ml penicillin, 100 μg/ml streptomycin, 2 mM L-glutamine, 100 μg/ml zeocin and 15 μg/ml blasticidin.

METHOD DETAILS

Cell cultures and treatments—RPE1 cells stably expressing DsRed-IRES-GFP, -GFP-Ala_6, or -GFP NS were selected using 0.8 mg/ml G418 (Sigma-Aldrich).

Cells inducibly expressing FLAG/HA-tagged NEMF wild-type were generated as described previously (Spitzer et al., 2013) and selected and maintained in media supplemented with 100 μg/ml hygromycin. Expression of tagged proteins was induced for 24 h by the addition of doxycycline at 1 μg/ml final concentration.

When indicated, cells were treated with 10 μM MG132 (Sigma-Aldrich) for 4 h, 20 μM Bortezomib (Fisher Scientific) for 6 h, or 1 μM MLN4924 (Biomol) for 5 h.

Transfection and siRNA knockdown—HeLa and RPE1 cells were transfected using Lipofectamine 3000 (Invitrogen) according to the manufacturer's protocol. For large-scale transfection of HeLa cells (15 cm dishes), PEI (polyethylenimine, 1 mg/ml) was used in a 1:3 ratio (DNA:PEI).

For knockdown experiments, HeLa and RPE1 cells were reverse transfected using RNAiMax (Invitrogen) according to the manufacturer's instructions. The following Silencer Select siRNA's (Invitrogen) were transfected at a final concentration of 10 nM for 72 hr: Silencer Select Negative Control No. 1 (4390843), Listerin (s25003), NEMF (s17483), Pirh2 (s24703), KLHDC10 (s22820), KLHDC2 (s24149), KLHDC3 (s41938) and UBE3C (s18659).

To generate RPE1 cells stably expressing DsRed-IRES-GFP, -GFP-Ala_6, or -GFP NS, RPE1 cells were electroporated with linearized plasmid using the Neon Transfection system (Thermo Fisher Scientific).

Plasmid construction—CRISPR cloning was performed by linearizing PX458 (a gift from Feng Zhang; Addgene plasmid #48138) using Bbs1 to insert annealed, phosphorylated gRNA oligos. Oligos were designed using the GPP Web Portal (https://portals.broadinstitute.org/gpp/public/analysis-tools/sgrna-design) and synthesized by Sigma-Aldrich.

pEGFP NS was generated by inverse PCR using pEGFP as a template, followed by phosphorylation and blunt ligation.

For C-terminally FLAG-tagged human NEMF constructs, the coding sequence was inserted into the pEGFP backbone using BamHI and NotI restriction sites. NEMF D96A R97A was generated by sequentially mutating residues Asp96 and Arg97 using site-directed mutagenesis PCR (Table S3).

For PAR-CLIP, NEMF cDNA was subcloned into pENTR4 (Thermo Fisher Scientific, A10465) plasmid for expression by adding attB1 and attB2 recombination sites to the primers followed by recombination using the Gateway BP recombinase (Thermo Fisher Scientific, 11789020). pENTR4 plasmids were recombined into the pFRT/TO/FLAG/HA-DEST destination vector (Thermo Fisher Scientific) using the Gateway LR recombinase (Thermo Fisher Scientific, 11791020). Further mutagenesis was performed using QuikChange Lightning Multi Site-Directed Mutagenesis Kit (Agilent) to obtain the mutants.

MSCV-CMV-DsRed-IRES-EGFP-DEST (a gift from Stephen Elledge; Addgene plasmid #41941) was sub-cloned into the pEGFP NS backbone using AgeI and BsrGI to generate DsRed-IRES-GFP NS. DsRed-IRES-GFP NS was linearized by SpeI digestion and used as a template to insert annealed oligos encoding the indicated degron sequences followed by a stop codon and a NotI restriction site (Table S4) using the In-Fusion kit (Takara Bio). Oligos were synthesized by Sigma-Aldrich.

Pirh2 and KLHDC2 were amplified from HeLa cell cDNA using gene-specific primers introducing 5' KpnI and 3' XhoI restriction sites in a two-step PCR (Table S3) and inserted into the pcDNA5 backbone containing an N-terminal 3xFLAG tag. Pirh2 M176E was generated using site-directed mutagenesis PCR (Table S3). KLHDC10 cDNA was subcloned from pCMV3-KLHDC10 (HG26504-UT, GenScript) into pcDNA5-3xFLAG using gene-specific primers introducing 5' HindIII and 3' XhoI restriction sites (Table S3).

For expression in BL21 cells, Pirh2 and KLHDC10 cDNA was subcloned into pET15b using primers introducing 5' NdeI and 3' XhoI restriction sites. The 6xHis tag was replaced by a GST tag using PCR and NcoI and NdeI restriction enzymes (Table S3). The codon-optimized, bicistronic insert encoding Elongin B (a.a. 1-104) and Elongin C (a.a. 1-112) was synthesized by Thermo Fisher and subcloned into pET28b using NdeI and SalI restriction sites.

Flow Cytometry—HeLa and RPE1 cells were trypsinized, washed once with PBS, re-suspended in 0.5 ml PBS, and kept on ice until data acquisition. Data was acquired on a FACSCanto instrument (BD Biosciences) with 488 nm and 561 nm lasers using the BD FACS Diva software. Untransfected cells were sorted out during acquisition. Data was analyzed using the FlowJo software. GFP levels were normalized to DsRed as an internal reference.

To generate monoclonal stable RPE1 cell lines, single cells were sorted into 96-well plates after antibiotic selection on a FACSAria III instrument (BD Biosciences).

Cell lysis—To analyze protein expression (Figures 4E, S1B, S1D, S4A, S4E-F, S5C and S6A-D), cells were washed once in ice-cold PBS and lysed in NP-40 buffer (20 mM TRIS pH 7.5, 150 mM NaCl, 5 mM EDTA, 0.5% NP-40, 1 mM DTT, supplemented with EDTA-free protease inhibitor tablet (Roche)) for 30 min at 4°C. Lysates were pre-cleared by centrifugation at 12,000 x g for 5 min at 4°C. Samples were boiled in 2x Laemmli buffer for 5 min at 95°C and analyzed by immunoblotting.

Immunoprecipitation—For interaction studies, GFP immunoprecipitations were performed from HeLa cells grown in 6 cm dishes. 24 hr after transfection with indicated plasmids (Figures 2E, 3B-E, 4A-B, S3A and S5A-B), cells were treated with 10 μM MG132 for 4 hr when necessary, washed in ice-cold PBS, and lysed in ice-cold ß-OG lysis buffer (20 mM TRIS pH 7.5, 100 mM KOAc, 5 mM $MgCl_2$, 1% ß-Octyl Glucoside (OG), 1 mM DTT, supplemented with EDTA-free protease inhibitor tablet (Roche)) for 30 min at 4°C. Lysates were pre-cleared by centrifugation at 12,000 x g for 5 min at 4°C. 10 μl GFP-Trap magnetic agarose beads (ChromoTek) were added to the pre-cleared lysates and rotated for 3 hr at 4°C. Beads were washed 3x in lysis buffer without DTT and proteins were eluted by boiling for 5 min at 95° in 2x Laemmli buffer for immunoblot analysis.

IP/LC-MS/MS and protein identification—Five 15-cm dishes of HeLa cells were transfected with GFP or GFP-Ala_6. 24 h after transfection, cells were treated with 10 μM MG132 for 4 hr and harvested in ice-cold ß-OG lysis buffer (composition described above). Lysates were incubated with 50 μl GFP-Trap magnetic agarose and rotated for 3 h at 4°C.

Beads were washed 3x in ß-OG lysis buffer without DTT, eluted with 0.2 M Glycine pH 2.5 and neutralized with 1 M TRIS pH 10.4. Samples were run on a 4-12% NuPAGE gel (Thermo Fisher Scientific) and stained using the Colloidal Blue Staining Kit (Invitrogen).

Gel slice regions containing proteins following colloidal blue staining, were in-gel digested with 300 ng trypsin (Pierce Biotechnology, Rockford, IL) for 3 h at 37°C using ProteaseMax™ Surfactant trypsin enhancer following reduction and alkylation with dithiothreitol and iodoacetamide, respectively, according to the manufacturer's instructions (Promega Corporation, Madison, WI). LC-MS/MS analysis of extracted peptides was subsequently carried out using an Orbitrap Fusion Tribrid mass spectrometer, following 2 µg capacity ZipTip (Millipore, Billeric, MA) C18 sample clean-up according to the manufacturer's instructions. Peptides were eluted from an Acclaim PepMap™ RSLC nano Viper analytical column (75-µm ID × 15 cm, Thermo Scientific, San Jose, CA) using a gradient of 5-25% solvent B (80/20 acetonitrile/water, 0.1% formic acid) in 90 min, followed by 25-44% solvent B in 30 min, 44-80% solvent B in 0.10 min, a 5 min hold of 80% solvent B, a return to 5% solvent B in 0.10 min, and finally a 20 min hold of solvent B. All flow rates were 300nL/min delivered using a nEasy-LC1000 nano liquid chromatography system (Thermo Fisher Scientific, San Jose, CA). Solvent A consisted of water and 0.1% formic acid. Ions were created at 1.8 kV using the Nanospray Flex™ ion source (Thermo Fisher Scientific, San Jose, CA). Data dependent scanning was performed by the Xcalibur v 4.0.27.10 software using a survey scan at 120,000 resolution in the Orbitrap analyzer scanning mass/charge (m/z) 380-2000 followed by higher-energy collisional dissociation (HCD) tandem mass spectrometry (MS/MS) at a normalized collision energy of 30 % of the most intense ions at maximum speed, at an automatic gain control of 1.0E4. Precursor ions were selected by the monoisotopic precursor selection (MIPS) setting to peptide and MS/MS was performed on charged species of 1-8 or 2-8 charges at a resolution of 30,000. Dynamic exclusion was set to exclude ions after two times within a 30 sec window, for 20 sec. Tandem mass spectra were searched against a human FASTA database of reviewed proteins from UniprotKB downloaded on March 03, 2017, to which additional common contaminant proteins (e.g., trypsin; obtained at ftp://ftp.thegpm.org/fasta/cRAP) were appended.

All MS/MS spectra were searched using Thermo Proteome Discoverer 1.4.1.14 (Thermo Fisher Scientific) considering fully tryptic peptides with up to 2 missed cleavage sites. Variable modifications considered during the search included methionine oxidation (15.995 Da), and cysteine carbamidomethylation (57.021 Da). At the time of the search, the protein database built as described above, contained 20,123 entries. Proteins were identified at 99 % confidence with XCorr score cut-offs (Qian et al., 2005) as determined by a reversed database search. The protein and peptide identification results were also visualized with Scaffold v 4.7.1 (Proteome Software Inc., Portland OR), a program that relies on various search engine results (*i.e.*: Sequest, X!Tandem, MASCOT) and which uses Bayesian statistics to reliably identify more spectra (Keller et al., 2002). Proteins were accepted that passed a minimum of two peptides identified at 0.1 % peptide and protein FDR, within Scaffold.

Semi-denaturing GFP pulldown—To detect GFP NS and GFP-Ala_6 ubiquitylation (Figures 1C, 4C and S5E), GFP immunoprecipitation was performed under semi-denaturing conditions. HeLa cells were grown on 15 cm dishes and treated with MG132 for 4 h before harvesting in ice-cold lysis buffer (20 mM TRIS pH 7.5, 150 mM NaCl, 0.5% Triton, 1 mM EDTA, 100 mM NEM (N-Ethylmaleimide), supplemented with EDTA-free protease inhibitor tablet (Roche)). After clarification, lysates were incubated with 20 μl GFP trap magnetic agarose and rotated for 3 h at 4°C. Beads were washed 1x in 10 mM TRIS pH 7.5, 150 mM NaCl, 0.5 mM EDTA, 100 mM NEM, supplemented with EDTA-free protease inhibitor tablet (Roche), 3x in stringent wash buffer (8 M UREA, 1% SDS in PBS), and 1x in 1% SDS/PBS. Proteins were eluted by boiling for 10 min at 95°C in 40 μl 2x Laemmli Buffer and analyzed by immunoblot.

Immunoblotting—Protein lysates were separated by SDS PAGE (4-20% Bis TRIS gel (GenScript)) and transferred to PVDF membrane (0.45 mm) for 1 h at 30 V using the Invitrogen Mini Blot Module (Invitrogen, USA). Proteins were detected using specific primary antibodies followed by incubation with HRP-conjugated secondary antibodies. Images were acquired with an LAS4000 instrument (GE ImageQuant) using chemiluminescence (ECL, GE Healthcare).

CRISPR-mediated knockout (KO)—Early-passage HeLa and RPE1 cells were grown to 70% confluency in 10 cm dishes and transfected with 20 μg PX458 plasmid encoding gRNA against either *LTN1* or *NEMF* using Lipofectamine 3000. After 24 h, cells were trypsinized and resuspended in PBS supplemented with 0.5% FBS. Cells were sorted using a BD FACSAria III instrument and analyzed with the BD FACSDiva software. The brightest 5% of GFP-positive cells were sorted into single cells/96-well and recovered after 7-12 days incubation at 37°C in High Survival Media (HSM, 20% log-phase conditioned media, supplemented with 20% FBS). HSM was mixed in DMEM (HeLa) or DMEM-F12 (RPE1). Monoclonal lines were expanded and screened by immunoblot using N-terminal antibodies against NEMF and Listerin. Validated KO clones were mapped for CRISPR mutation by extracting gDNA using DirectPCR® (Viagen), amplifying the relevant exon by PCR (Table S3) and TOPO™ TA Cloning™ (Invitrogen) the PCR product for Sanger sequencing (Eurofins GATC).

HeLa LTN1 KO (LKO) cell line holds an insertion of T after G12298 and a deletion of 17 bp from T12289 to C12305 in exon 6 of the *LTN1* gene (ENSG00000198862, GRCH38.p13). HeLa NEMF KO (NKO) cell line holds an A1830 deletion and a 5-bp deletion from A1830 to T1834 in exon 3 of the *NEMF* gene (ENSG00000165525, GRCH38.p13). HeLa LTN1/NEMF KO (LNKO) cell line was derived from HeLa NKO and holds a G12298/T12299 deletion and a 5-bp deletion from C12295 to T12299 in exon 6 of the *LTN1* gene. RPE1 LKO cell line holds an insertion of T after G12298 and a 171-bp insertion after T12300 in exon 6 of the *LTN1* gene.

All CRISPR induced indels result in early or immediate termination of the protein. Deletion of A1830 and A1830-T1834 in *NEMF* in HeLa NKO and LNKO cells appends 1 and 3 amino acids after NEMF K67, respectively, followed by an in-frame stop codon. Insertion of T after G12298 and deletion of T12289 in *LTN1* in HeLa LKO cells append 16 and 14

amino acids after Listerin V224 and K220, respectively, followed by an in-frame stop codon. Deletion of G12298-T12299 and C12295-T12299 in *LTN1* in HeLa LNKO cells append 16 amino acids after Listerin R223 and Y222, respectively, followed by an in-frame stop codon. Insertion of T after G12298 in *LTN1* in RPE1 LKO cells appends 16 amino acids after Listerin V224 followed by an in-frame stop codon. Insertion of 171 bp's after T12300 in *LTN1* in RPE1 LKO cells appends 40 amino acids after Listerin V224 followed by an in-frame stop codon.

qPCR—RNA was extracted from 12-well (HeLa) or 6-well (RPE1) plates using the RNeasy Mini Kit (Qiagen). 1 μg RNA was reverse transcribed using the QuantiTect Reverse Transcription Kit (Qiagen) according to the manufacturer's instructions. qPCR was performed in technical triplicates using the LightCycler 480 SYBR Green I Master mix (Roche) in a 15 μl reaction and the Light Cycler 480 II instrument (Roche). 45 cycles of the following program were run: 10 sec at 95°C, 10 sec at 62°C, 10 sec at 72°C. qPCR primers were designed using the IDTDNA PrimerQuest Tool. Primer sequences are listed in Table S5. mRNA levels were normalized to the expression of 5S rRNA and relative fold changes were calculated using the ΔΔCt method.

Purification of recombinant proteins—GST-Pirh2 was expressed in *E. coli* strain BL21 (DE3) grown in LB media with Ampicillin (100 μg/ml) for 4 h at 30°C after induction with 1 mM IPTG. Cells were lysed by sonication (Hielscher, UP100H) in ice-cold buffer (50 mM TRIS pH 7.5, 150 mM NaCl, 0.5% NP40, 1 mM DTT, supplemented with EDTA-free protease inhibitor (Roche)). Pre-cleared lysates were incubated with GST bead-slurry (Machery-Nagel) and rotated for 30 min at RT. Beads were washed three times in ice-cold lysis buffer without DTT. GST-Pirh2 was eluted with 10 mM reduced Glutathione (Sigma-Aldrich) for 15 min at RT and supplemented with glycerol at final concentration of 10% (w/v).

GST-KLHDC10, Elongin B and Elongin C were co-expressed in *E. coli* BL21 (DE3) cells. Cells were grown in LB media supplemented with Ampicillin (100 μg/ml) and Kanamycin (50 μg/ml) at 37°C until OD 0.6. Protein expression was carried out overnight at 18°C by adding 0.75 mM IPTG. Cells were lysed by sonication in ice-cold buffer (50 mM TRIS pH 7.5, 150 mM NaCl, 1 mM DTT, 0.5% Triton X-100 and EDTA-free protease inhibitor (Roche)). GST-KLHDC10 was purified using GST beads as described above.

GFP, GFP-Ala_6 and GFP-Thr_6 were purified from a *B. subtilis ΔclpP* strain as described previously (Lytvynenko et al., 2019). Cells were grown in LB medium at 37°C, harvested at OD 2.0, and lysed as described above. After clarification, lysates were incubated with GFP-Trap agarose slurry (ChromoTek) and rotated for 1 h at 4°C. The beads were washed three times in lysis buffer without DTT and GFP or GFP-Ala_6 were eluted with 0.2 M Glycine pH 2.5 for 10 min at 4°C. The pH was neutralized using 1 M TRIS pH 10.4, and glycerol was added to a final concentration of 10% (w/v).

***In vitro* binding assay—**Direct interaction of GFP-Ala_6 and GST-Pirh2 or GST-KLHDC10 (Figure S3B) was assessed using recombinant proteins purified from *E. coli*. GST agarose beads (Machery-Nagel) were washed in assay buffer (20 mM TRIS pH 7.5,

100 mM NaCl, 0.1% Tween-20) and blocked using assay buffer supplemented with 1% BSA for 2 h at 4°C. GST beads were then incubated with 10 μg purified GST-Pirh2 or GST-KLHDC10 in 100 μl assay buffer for 2 h at 4°C. Beads were washed twice in assay buffer and incubated with 0.25 μg GFP, GFP-Ala_6 or GFP-Thr_6 in 100 μl assay buffer supplemented with 1% BSA for 1 h at 4°C. Following 3 washes in assay buffer, proteins were eluted from the beads by boiling for 5 min at 95°C in Laemmli buffer for immunoblot analysis.

***In vitro* ubiquitylation assay—**To detect GFP-Ala_6 ubiquitylation (Figure S3C), 50 ng E1 enzyme (mouse UBA1), 100 ng E2 enzyme (human UBE2D2), 5 μg ubiquitin (Sigma-Aldrich), 1 μg GST-Pirh2 and 1 μg GFP or GFP-Ala_6 were incubated at 30°C for 90 min in ubiquitylation buffer (50 mM TRIS pH 7.6, 5 mM $MgCl_2$, 2 mM ATP, 2 mM DTT). The reaction was stopped by adding 2x Laemmli buffer and boiling for 5 min at 95°C. Proteins were separated on a 4-20 % Bis-TRIS gel and ubiquitylation was detected by immunoblot.

QUANTIFICATION AND STATISTICAL ANALYSIS

PAR-CLIP—For PAR-CLIP analysis Flp-In™ T-REx™ 293 cells expressing FLAG-HA-tagged NEMF were used. PAR-CLIP was performed using a single RNase A digestion step and anti-FLAG-M2 magnetic beads (Sigma-Aldrich) for immunoprecipitation as described previously (Garzia et al., 2017b). PAR-CLIP cDNA libraries were sequenced on an Illumina HiSeq 2500 instrument, and data were analyzed using the PAR-CLIP suite (Garzia et al., 2017b), allowing up to 2 mismatches. Reads mapping to tRNAs with a T-to-C mismatch and ≥20 nt were extracted and mapped to reference tRNAs. A substantial fraction of reads mapping to tRNA-Ala could not map with 1 or 2 mismatches and appeared to skip 1-2 nucleotides in positions 23-26, the region where m2G modification might happen and impact the reverse transcription reaction. We repeated the mapping allowing gaps which was later compared to the tRNA sequencing dataset (Gogakos et al., 2017) obtained by HydroSeq (Karaca et al., 2014) for differential expression. The analysis was conducted with the R/Bioconductor package edgeR (Robinson et al., 2010) v. 3.14.0. The read counts were normalized using the weighted trimmed mean of M values (Robinson and Oshlack, 2010) and normalized for library size. The differences were tested using the exact test and the read count variation was estimated using tagwise or common dispersion. Differences were considered significant below a false discovery rate (FDR) of 5%.

Statistical analysis—Statistical analysis details and significance reports can be found in corresponding figures and figure legends. P values < 0.05 were considered significant. All statistical analysis was performed using GraphPad Prism 8.

Supplementary Material

Refer to Web version on PubMed Central for supplementary material.

ACKNOWLEDGMENTS

We thank Manuel Kaulich, Danny Huang, and Frauke Melchior for providing the RPE1 cell line, recombinant UBE2D2 protein, and the UBA1 plasmid, respectively. We also thank Adam Hlaváček (Joazeiro laboratory) for E1 protein, George Tsaprailis (Scripps Florida Proteomics Facility) for mass spectrometry analyses, the ZMBH FACS

Facility, Rick Maser from the JAX Genetic Engineering Technologies group, and the Joazeiro laboratory for discussions. Work in the Joazeiro laboratory is supported in part by the Deutsche Forschungsgemeinschaft (DFG, German Research Foundation) Project 201348542 (SFB 1036) and by the National Institute of Neurological Disorders and Stroke (NINDS) of the NIH (R01 NS102414).

REFERENCES

BENGTSON MH & JOAZEIRO CA 2010. Role of a ribosome-associated E3 ubiquitin ligase in protein quality control. Nature, 467, 470–3. [PubMed: 20835226]

BRANDMAN O, STEWART-ORNSTEIN J, WONG D, LARSON A, WILLIAMS CC, LI GW, ZHOU S, KING D, SHEN PS, WEIBEZAHN J, DUNN JG, ROUSKIN S, INADA T, FRoSt A & WEISSMAN JS 2012. A ribosome-bound quality control complex triggers degradation of nascent peptides and signals translation stress. Cell, 151, 1042–54. [PubMed: 23178123]

BURROUGHS AM & ARAVIND L 2014. A highly conserved family of domains related to the DNA-glycosylase fold helps predict multiple novel pathways for RNA modifications. RNA Biol, 11, 360–72. [PubMed: 24646681]

CHANDRASEKARAN V, JUSZKIEWICZ S, CHOI J, PUGLISI JD, BROWN A, SHAO S, RAMAKRISHNAN V & HEGDE RS 2019. Mechanism of ribosome stalling during translation of a poly(A) tail. Nat Struct Mol Biol, 26, 1132–1140. [PubMed: 31768042]

CHOE YJ, PARK SH, HASSEMER T, KORNER R, VINCENZ-DONNELLY L, HAYER-HARTL M & HARTL FU 2016. Failure of RQC machinery causes protein aggregation and proteotoxic stress. Nature, 531, 191–5. [PubMed: 26934223]

CHU J, HONG NA, MASUDA CA, JENKINS BV, NELMS KA, GOODNOW CC, GLYNNE RJ, WU H, MASLIAH E, JOAZEIRO CA & KAY SA 2009. A mouse forward genetics screen identifies LISTERIN as an E3 ubiquitin ligase involved in neurodegeneration. Proc Natl Acad Sci U S A, 106, 2097–103. [PubMed: 19196968]

CROWE-MCAULIFFE C, TAKADA H, MURINA V, POLTE C, KASVANDIK S, TENSON T, IGNATOVA Z, ATKINSON GC, WILSON DN & HAURYLIUK V 2021. Structural Basis for Bacterial Ribosome-Associated Quality Control by RqcH and RqcP. Mol Cell, 81, 115–126 e7. [PubMed: 33259810]

DEFENOUILLERE Q & FROMONT-RACINE M 2017. The ribosome-bound quality control complex: from aberrant peptide clearance to proteostasis maintenance. Curr Genet, 63, 997–1005. [PubMed: 28528489]

DEFENOUILLERE Q, YAO Y, MOUAIKEL J, NAMANE A, GALOPIER A, DECOURTY L, DOYEN A, MALABAT C, SAVEANU C, JACQUIER A & FROMONT-RACINE M 2013. Cdc48-associated complex bound to 60S particles is required for the clearance of aberrant translation products. Proc Natl Acad Sci U S A, 110, 5046–51. [PubMed: 23479637]

DEFENOUILLERE Q, ZHANG E, NAMANE A, MOUAIKEL J, JACQUIER A & FROMONT-RaCiNE M 2016. Rqc1 and Ltn1 Prevent C-terminal Alanine-Threonine Tail (CAT-tail)-induced Protein Aggregation by Efficient Recruitment of Cdc48 on Stalled 60S Subunits. J Biol Chem, 291, 12245–53. [PubMed: 27129255]

DOBIN A, DAVIS CA, SCHLESINGER F, DRENKOW J, ZALESKI C, JHA S, BATUT P, CHAISSON M & GINGERAS TR 2013. STAR: ultrafast universal RNA-seq aligner. Bioinformatics, 29, 15–21. [PubMed: 23104886]

FANG NN, NG AH, MEASDAY V & MAYOR T 2011. Hul5 HECT ubiquitin ligase plays a major role in the ubiquitylation and turnover of cytosolic misfolded proteins. Nat Cell Biol, 13, 1344–52. [PubMed: 21983566]

FILBECK S, CERULLO F, PATERNOGA H, TSAPRAILIS G, JOAZEIRO CAP & PFEFFER S 2021. Mimicry of Canonical Translation Elongation Underlies Alanine Tail Synthesis in RQC. Mol Cell, 81, 104–114 e6. [PubMed: 33259811]

FINLEY D 2011. Misfolded proteins driven to destruction by Hul5. Nat Cell Biol, 13, 1290–2. [PubMed: 21983564]

GARZIA A, JAFARNEJAD SM, MEYER C, CHAPAT C, GOGAKOS T, MOROZOV P, AMIRI M, SHAPIRO M, MOLINA H, TUSCHL T & SONENBERG N 2017a. The E3 ubiquitin ligase and

RNA-binding protein ZNF598 orchestrates ribosome quality control of premature polyadenylated mRNAs. Nat Commun, 8, 16056. [PubMed: 28685749]

GARZIA A, MEYER C, MOROZOV P, SAJEK M & TUSCHL T 2017b. Optimization of PAR-CLIP for transcriptome-wide identification of binding sites of RNA-binding proteins. Methods, 118–119, 24–40.

GOGAKOS T, BROWN M, GARZIA A, MEYER C, HAFNER M & TUSCHL T 2017. Characterizing Expression and Processing of Precursor and Mature Human tRNAs by Hydro-tRNAseq and PAR-CLIP. Cell Rep, 20, 1463–1475. [PubMed: 28793268]

JOAZEIRO CAP 2019. Mechanisms and functions of ribosome-associated protein quality control. Nat Rev Mol Cell Biol, 20, 368–383. [PubMed: 30940912]

JUSZKIEWICZ S & HEGDE RS 2017. Initiation of Quality Control during Poly(A) Translation Requires Site-Specific Ribosome Ubiquitination. Mol Cell, 65, 743–750 e4. [PubMed: 28065601]

KARACA E, WEITZER S, PEHLIVAN D, SHIRAISHI H, GOGAKOS T, HANADA T, JHANGIANI SN, WISZNIEWSKI W, WITHERS M, CAMPBELL IM, ERDIN S, ISIKAY S, FRANCO LM, GONZAGA-JAUREGUI C, GAMBIN T, GELOWANI V, HUNTER JV, YESIL G, KOPARIR E, YILMAZ S, BROWN M, BRISKIN D, HAFNER M, MOROZOV P, FARAZI TA, BERNREUTHER C, GLATZEL M, TRATTNIG S, FRISKE J, KRONNERWETTER C, BAINBRIDGE MN, GEZDIRICI A, SEVEN M, MUZNY DM, BOERWINKLE E, OZEN M, BAYLOR HOPKINS CENTER FOR MENDELIAN, G., CLAUSEN T, TUSCHL T, YUKSEL A, HESS A, GIBBS RA, MARTINEZ J, PENNINGER JM & LUPSKI JR 2014. Human CLP1 mutations alter tRNA biogenesis, affecting both peripheral and central nervous system function. Cell, 157, 636–50. [PubMed: 24766809]

KELLER A, NESVIZHSKII AI, KOLKER E & AEBERSOLD R 2002. Empirical statistical model to estimate the accuracy of peptide identifications made by MS/MS and database search. Anal Chem, 74, 5383–92. [PubMed: 12403597]

KOREN I, TIMMS RT, KULA T, XU Q, LI MZ & ELLEDGE SJ 2018. The Eukaryotic Proteome Is Shaped by E3 Ubiquitin Ligases Targeting C-Terminal Degrons. Cell, 173, 1622–1635 e14. [PubMed: 29779948]

KOSTOVA KK, HICKEY KL, OSUNA BA, HUSSMANN JA, FROST A, WEINBERG DE & WEISSMAN JS 2017. CAT-tailing as a fail-safe mechanism for efficient degradation of stalled nascent polypeptides. Science, 357, 414–417. [PubMed: 28751611]

KUROHA K, ZINOVIEV A, HELLEN CUT & PESTOVA TV 2018. Release of Ubiquitinated and Non-ubiquitinated Nascent Chains from Stalled Mammalian Ribosomal Complexes by ANKZF1 and Ptrh1. Mol Cell, 72, 286–302 e8. [PubMed: 30244831]

LENG RP, LIN Y, MA W, WU H, LEMMERS B, CHUNG S, PARANT JM, LOZANO G, HAKEM R & BENCHIMOL S 2003. Pirh2, a p53-induced ubiquitin-protein ligase, promotes p53 degradation. Cell, 112, 779–91. [PubMed: 12654245]

LIN HC, YEH CW, CHEN YF, LEE TT, HSIEH PY, RUSNAC DV, LIN SY, ELLEDGE SJ, ZHENG N & YEN HS 2018. C-Terminal End-Directed Protein Elimination by CRL2 Ubiquitin Ligases. Mol Cell, 70, 602–613 e3. [PubMed: 29775578]

LUH LM & BERTOLOTTI A 2020. Potential benefit of manipulating protein quality control systems in neurodegenerative diseases. Curr Opin Neurobiol, 61, 125–132. [PubMed: 32199101]

LYTVYNENKO I, PATERNOGA H, THRUN A, BALKE A, MULLER TA, CHIANG CH, NAGLER K, TSAPRAILIS G, ANDERS S, BISCHOFS I, MAUPIN-FURLOW JA, SPAHN CMT & JOAZEIRO CAP 2019. Alanine Tails Signal Proteolysis in Bacterial Ribosome-Associated Quality Control. Cell, 178, 76–90 e22. [PubMed: 31155236]

LYUMKIS D, OLIVEIRA DOS PASSOS D, TAHARA EB, WEBB K, BENNETT EJ, VINTERBO S, POTTER CS, CARRAGHER B & JOAZEIRO CA 2014. Structural basis for translational surveillance by the large ribosomal subunit-associated protein quality control complex. Proc Natl Acad Sci U S A, 111, 15981–6. [PubMed: 25349383]

MACHNICKA MA, MILANOWSKA K, OSMAN OGLOU O, PURTA E, KURKOWSKA M, OLCHOWIK A, JANUSZEWSKI W, KALINOWSKI S, DUNIN-HORKAWICZ S, ROTHER KM, HELM M, BUJNICKI JM & GROSJEAN H 2013. MODOMICS: a database of RNA modification pathways--2013 update. Nucleic Acids Res, 41, D262–7. [PubMed: 23118484]

MARTIN PB, KIGOSHI-TANSHO Y, SHER RB, RAVENSCROFT G, STAUFFER JE, KUMAR R, YONASHIRO R, MULLER T, GRIFFITH C, ALLEN W, PEHLIVAN D, HARAL T, ZENKER M, HOWTING D, SCHANZE D, FAQEIH EA, ALMONTASHIRI NAM, MAROOFIAN R, HOULDEN H, MAZAHERI N, GALEHDARI H, DOUGLAS G, POSEY JE, RYAN M, LUPSKI JR, LAING NG, JOAZEIRO CAP & COX GA 2020. NEMF mutations that impair ribosome-associated quality control are associated with neuromuscular disease. Nat Commun, 11, 4625. [PubMed: 32934225]

OSUNA BA, HOWARD CJ, KC S, FROST A & WEINBERG DE 2017. In vitro analysis of RQC activities provides insights into the mechanism and function of CAT tailing. Elife, 6:e27949. [PubMed: 28718767]

PISAREVA VP, SKABKIN MA, HELLEN CU, PESTOVA TV & PISAREV AV 2011. Dissociation by Pelota, Hbs1 and ABCE1 of mammalian vacant 80S ribosomes and stalled elongation complexes. EMBO J, 30, 1804–17. [PubMed: 21448132]

POHL C & DIKIC I 2019. Cellular quality control by the ubiquitin-proteasome system and autophagy. Science, 366, 818–822. [PubMed: 31727826]

PRAKASH S, TIAN L, RATLIFF KS, LEHOTZKY RE & MATOUSCHEK A 2004. An unstructured initiation site is required for efficient proteasome-mediated degradation. Nat Struct Mol Biol, 11, 830–7. [PubMed: 15311270]

QIAN WJ, LIU T, MONROE ME, STRITTMATTER EF, JACOBS JM, KANGAS LJ, PETRITIS K, CAMP DG 2ND & SMITH RD 2005. Probability-based evaluation of peptide and protein identifications from tandem mass spectrometry and SEQUEST analysis: the human proteome. J Proteome Res, 4, 53–62. [PubMed: 15707357]

ROBINSON MD, MCCARTHY DJ & SMYTH GK 2010. edgeR: a Bioconductor package for differential expression analysis of digital gene expression data. Bioinformatics, 26, 139–40. [PubMed: 19910308]

ROBINSON MD & OSHLACK A 2010. A scaling normalization method for differential expression analysis of RNA-seq data. Genome Biol, 11, R25. [PubMed: 20196867]

ROSS CA & POIRIER MA 2004. Protein aggregation and neurodegenerative disease. Nat Med, 10 Suppl, S10–7. [PubMed: 15272267]

RUSNAC DV, LIN HC, CANZANI D, TIEN KX, HINDS TR, TSUE AF, BUSH MF, YEN HS & ZHENG N 2018. Recognition of the Diglycine C-End Degron by CRL2(KLHDC2) Ubiquitin Ligase. Mol Cell, 72, 813–822 e4. [PubMed: 30526872]

SAITO S, HOSODA N & HOSHINO S 2013. The Hbs1-Dom34 protein complex functions in non-stop mRNA decay in mammalian cells. J Biol Chem, 288, 17832–43. [PubMed: 23667253]

SEKINE Y, HATANAKA R, WATANABE T, SONO N, IEMURA S, NATSUME T, KURANAGA E, MIURA M, TAKEDA K & ICHIJO H 2012. The Kelch repeat protein KLHDC10 regulates oxidative stress-induced ASK1 activation by suppressing PP5. Mol Cell, 48, 692–704. [PubMed: 23102700]

SHAO S, BROWN A, SANTHANAM B & HEGDE RS 2015. Structure and assembly pathway of the ribosome quality control complex. Mol Cell, 57, 433–44. [PubMed: 25578875]

SHAO S & HEGDE RS 2014. Reconstitution of a minimal ribosome-associated ubiquitination pathway with purified factors. Mol Cell, 55, 880–890. [PubMed: 25132172]

SHAO S, VON DER MALSBURG K & HEGDE RS 2013. Listerin-dependent nascent protein ubiquitination relies on ribosome subunit dissociation. Mol Cell, 50, 637–48. [PubMed: 23685075]

SHEN PS, PARK J, QIN Y, LI X, PARSAWAR K, LARSON MH, COX J, CHENG Y, LAMBOWITZ AM, WEISSMAN JS, BRANDMAN O & FROST A 2015. Protein synthesis. Rqc2p and 60S ribosomal subunits mediate mRNA-independent elongation of nascent chains. Science, 347, 75–8. [PubMed: 25554787]

SHENG Y, LAISTER RC, LEMAK A, WU B, TAI E, DUAN S, LUKIN J, SUNNERHAGEN M, SRISAILAM S, KARRA M, BENCHIMOL S & ARROWSMITH CH 2008. Molecular basis of Pirh2-mediated p53 ubiquitylation. Nat Struct Mol Biol, 15, 1334–42. [PubMed: 19043414]

SHOEMAKER CJ, EYLER DE & GREEN R 2010. Dom34:Hbs1 promotes subunit dissociation and peptidyl-tRNA drop-off to initiate no-go decay. Science, 330, 369–72. [PubMed: 20947765]

SITRON CS & BRANDMAN O 2019. CAT tails drive degradation of stalled polypeptides on and off the ribosome. Nat Struct Mol Biol, 26, 450–459. [PubMed: 31133701]

SOUCY TA, SMITH PG, MILHOLLEN MA, BERGER AJ, GAVIN JM, ADHIKARI S, BROWNELL JE, BURKE KE, CARDIN DP, CRITCHLEY S, CULLIS CA, DOUCETTE A, GARNSEY JJ, GAULIN JL, GERSHMAN RE, LUBLINSKY AR, MCDONALD A, MIZUTANI H, NARAYANAN U, OLHAVA EJ, PELUSO S, REZAEI M, SINTCHAK MD, TALREJA T, THOMAS MP, TRAORE T, VYSKOCIL S, WEATHERHEAD GS, YU J, ZHANG J, DICK LR, CLAIBORNE CF, ROLFE M, BOLEN JB & LANGSTON SP 2009. An inhibitor of NEDD8-activating enzyme as a new approach to treat cancer. Nature, 458, 732–6. [PubMed: 19360080]

SPITZER J, LANDTHALER M & TUSCHL T 2013. Rapid creation of stable mammalian cell lines for regulated expression of proteins using the Gateway(R) recombination cloning technology and Flp-In T-REx(R) lines. Methods Enzymol, 529, 99–124. [PubMed: 24011039]

TOMITA T & MATOUSCHEK A 2019. Substrate selection by the proteasome through initiation regions. Protein Sci, 28, 1222–1232. [PubMed: 31074920]

VARSHAVSKY A 2019. N-degron and C-degron pathways of protein degradation. Proc Natl Acad Sci U S A, 116, 358–366. [PubMed: 30622213]

VERMA R, REICHERMEIER KM, BURROUGHS AM, OANIA RS, REITSMA JM, ARAVIND L & DESHAIES RJ 2018. Vms1 and ANKZF1 peptidyl-tRNA hydrolases release nascent chains from stalled ribosomes. Nature, 557, 446–451. [PubMed: 29632312]

VON DER MALSBURG K, SHAO S & HEGDE RS 2015. The ribosome quality control pathway can access nascent polypeptides stalled at the Sec61 translocon. Mol Biol Cell, 26, 2168–80. [PubMed: 25877867]

YEN HC, XU Q, CHOU DM, ZHAO Z & ELLEDGE SJ 2008. Global protein stability profiling in mammalian cells. Science, 322, 918–23. [PubMed: 18988847]

YIP MCJ, KESZEI AFA, FENG Q, CHU V, MCKENNA MJ & SHAO S 2019. Mechanism for recycling tRNAs on stalled ribosomes. Nat Struct Mol Biol, 26, 343–349. [PubMed: 31011209]

YONASHIRO R, TAHARA EB, BENGTSON MH, KHOKHRINA M, LORENZ H, CHEN KC, KIGOSHI-TANSHO Y, SAVAS JN, YATES JR, KAY SA, CRAIG EA, MOGK A, BUKAU B & JOAZEIRO CA 2016. The Rqc2/Tae2 subunit of the ribosome-associated quality control (RQC) complex marks ribosome-stalled nascent polypeptide chains for aggregation. Elife, 5, e11794. [PubMed: 26943317]

Highlights

- Mammalian Rqc2 (NEMF) can target RQC substrates for degradation independently of Listerin
- NEMF binds tRNA-Ala to modify 60S-obstructing polypeptides with C-terminal alanine tails
- The Ala-tail modification is sensed by the C-end rule E3 ligases, $CRL2^{KLHDC10}$ and Pirh2
- The results also uncover a role for the C-end rule pathway in protein quality control

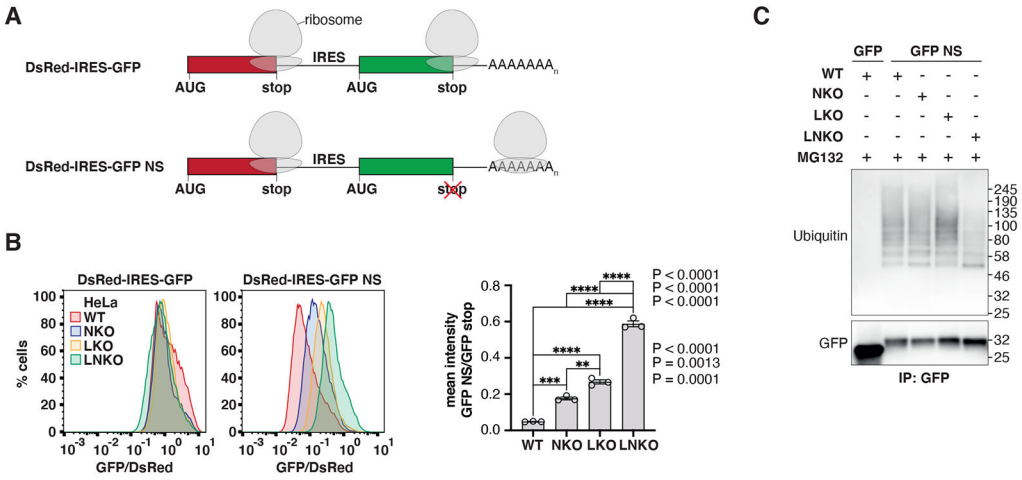

Figure 1. NEMF promotes Listerin-independent degradation of non-stop proteins in mammalian cells

(A) Schematic diagram of mRNA encoded by bicistronic reporter constructs with DsRed and GFP being translated, and indicating a ribosome translating past the GFP coding sequence and into the poly(A) tail in the non-stop (NS) mRNA.

(B) HeLa cells were transiently transfected with DsRed-IRES-GFP or -GFP NS and analyzed by flow cytometry. Stability of the reporter was assessed by normalizing GFP to DsRed fluorescence. Flow cytometry data was quantified from independent experiments (n = 3) and is represented as mean ± SEM. Ratios of mean GFP and DsRed fluorescence from cells expressing DsRed-IRES-GFP NS were normalized to mean GFP/DsRed ratios from cells expressing DsRed-IRES-GFP. Statistical analysis was performed using ordinary one-way ANOVA, P values are indicated.

(C) Ubiquitylation analysis of GFP NS from indicated cell lysates by semi-denaturing GFP IP followed by the indicated immunoblot. Quantification of independent experiments (n = 4) shows a 75% reduction in the GFP NS ubiquitylation signal from LNKO cells compared to LKO.

IRES, internal ribosomal entry site; WT, wild type; KO, knockout; NKO, NEMF KO; LKO, LTN1 KO; LNKO, LTN1/NEMF KO; NS, non-stop; WCL, whole cell lysate; IP, immunoprecipitation.

See also Figure S1.

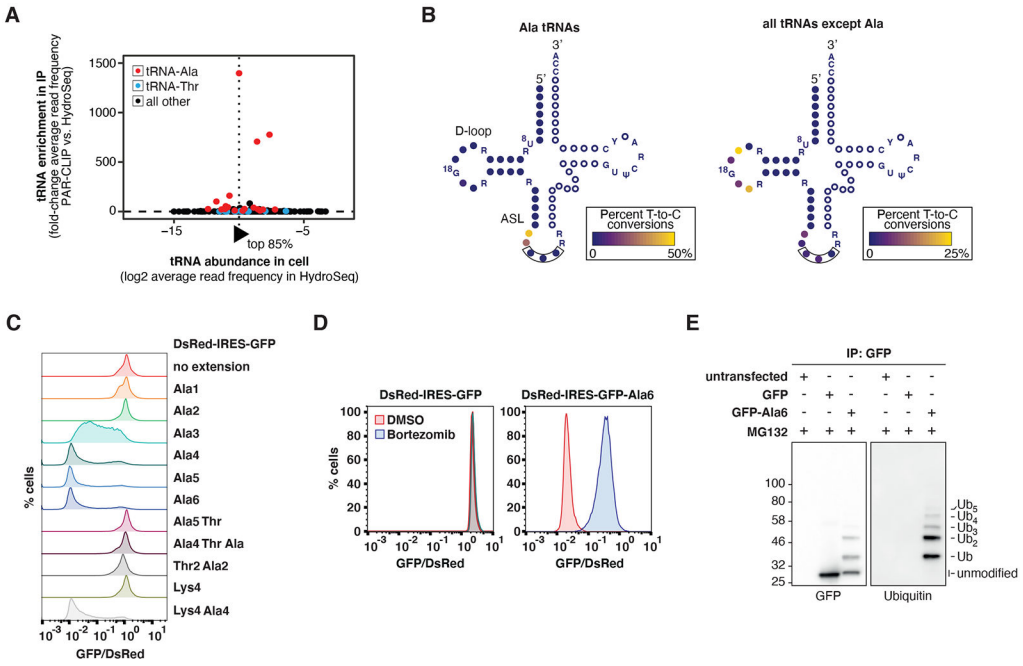

Figure 2. C-terminal Ala tails trigger ubiquitylation and proteasomal degradation

(A) Selective tRNA-Ala(IGC) enrichment by NEMF PAR-CLIP. *x-axis:* log2 average tRNA abundance in the cell (HydroSeq); *y-axis:* relative fold-changes in tRNA abundance in NEMF crosslinked reads (PAR-CLIP) compared to abundance in cell (HydroSeq). tRNA-Ala variants are colored in red, tRNA-Thr in blue, all other tRNAs in black.

(B) Schematic diagrams of tRNA secondary structure (*ASL*, anticodon stem-loop). To identify NEMF crosslinking sites on tRNAs, the efficiency (%) of T-to-C conversion resulting from PAR-CLIP crosslinking was calculated for individual positions of tRNA-Ala (*left*) and all other tRNAs together except tRNA-Ala (*right*). Conserved nucleotides across tRNAs are indicated by letters or symbols (*R=A/G; Y=C/T;* Ψ*=pseudouridine*), non-conserved nucleotides are depicted as circles. Filled circles represent nucleotides covered with high frequency by NEMF PAR-CLIP sequence reads.

(C) Flow cytometry analysis of HeLa cells transiently transfected with DsRed-IRES-GFP reporter constructs C-terminally fused to the indicated sequences.

(D) RPE1 cells stably expressing DsRed-IRES-GFP or -GFP-Ala_6 were treated or not with the proteasome inhibitor Bortezomib (20 μM for 6 h) and analyzed using flow cytometry. DMSO was used as a control vehicle.

(E) HeLa cells expressing GFP or GFP-Ala_6 were treated with the proteasome inhibitor MG132 (10 μM for 4 h) and subjected to GFP IP followed by immunoblot analysis to monitor ubiquitylation.

Ub, ubiquitin.

See also Figure S2.

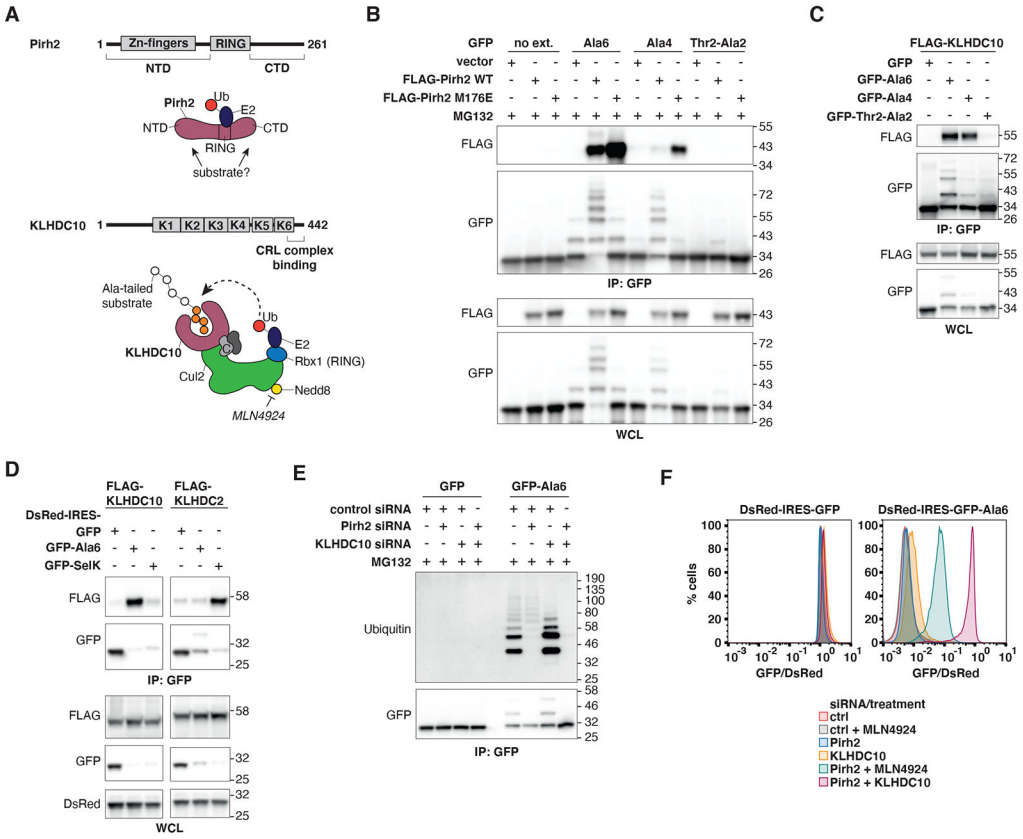

Figure 3. C-terminal Ala tails are recognized by Pirh2 and KLHDC10

(A) *Top*: schematic and cartoon diagrams of the domain arrangement of Pirh2; *bottom*: schematic diagram of the domain arrangement of KLHDC10 and cartoon representation of the subunit organization of the $CRL2^{KLHDC10}$ complex (Sekine et al., 2012). The E3 ligases are shown bound to Ub-conjugated E2, and KLHDC10 is also shown bound to an Ala-tailed (orange) substrate.

(B) The interaction of GFP, GFP-Ala_6, GFP-Ala_4 or GFP-Thr_2-Ala_2 with FLAG-tagged Pirh2 WT or the catalytically-inactive mutant M176E in MG132-treated HeLa cells was analyzed by GFP IP followed by anti-FLAG immunoblot.

(C) The interaction of GFP, GFP-Ala_6, GFP-Ala_4 or GFP-Thr_2-Ala_2 and FLAG-tagged KLHDC10 was analyzed as in “B”, but in the absence of MG132.

(D) Interaction of GFP-Ala_6 or GFP-SelK (a substrate of KLHDC2 ending in -GlyGly (Rusnac et al., 2018)) and FLAG-tagged KLHDC10 or KLHDC2 analyzed as in “C”.

(E) HeLa cells transiently transfected with GFP reporters were treated with Pirh2 and/or KLHDC10 siRNA and MG132. Ubiquitylation of GFP-Ala_6 was analyzed by GFP IP followed by immunoblot.

(F) RPE1 cells stably expressing GFP fusion reporters were treated with siRNAs targeting Pirh2 and/or KLHDC10 and with the Neddylation inhibitor MLN4924 (see “A”; 1 μM for 5 h) as indicated.

NTD, N-terminal domain; CTD, C-terminal domain; K1-6, Kelch repeats 1-6; CRL, Cullin-RING ligase; SelK, Selenoprotein K.

See also Figures S3, S4, S7 and Table S1.

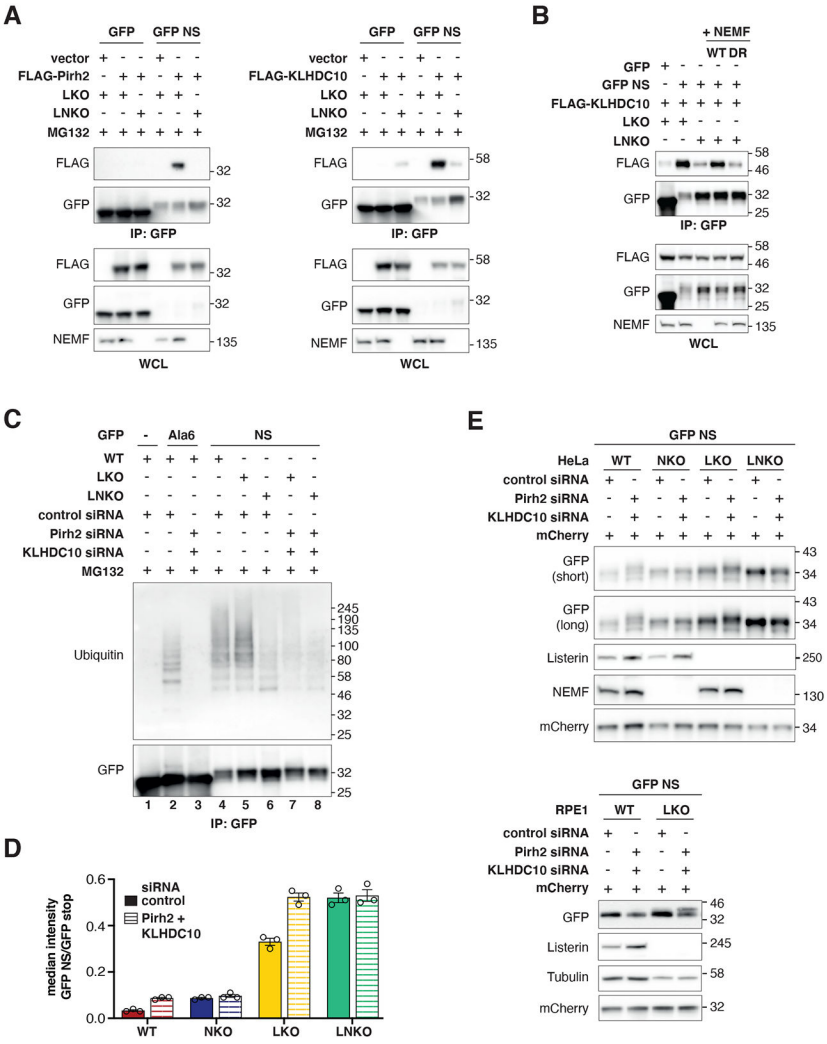

Figure 4. Pirh2 and KLHDC10 promote degradation of non-stop proteins in a NEMF-dependent manner

(A) HeLa LKO or LNKO cells expressing GFP or GFP NS and FLAG-tagged Pirh2 or KLHDC10 were treated with MG132 (10 μM for 4 h). Interaction of GFP NS with the E3 ligases was analyzed by GFP IP followed by anti-FLAG immunoblot.

(B) Interaction between GFP NS and KLHDC10 was analyzed in the presence or absence of NEMF WT or the catalytically inactive mutant D96A/R97A (DR) as described in “A”, but in the absence of MG132.

(C) Different cell lines expressing GFP, GFP-Ala_6 or GFP-NS were treated with control, Pirh2 and/or KLHDC10 siRNA, as indicated. Ubiquitylation levels of GFP NS were assessed by semi-denaturing GFP IP and anti-ubiquitin immunoblot.

(D) Effect of Pirh2 and KLHDC10 depletion on GFP NS stability in HeLa WT, NKO, LKO, and LNKO cell lines. Cells were knocked down with control or Pirh2 and KLHDC10 siRNA followed by transfection with DsRed-IRES-GFP or -GFP NS. GFP and DsRed fluorescence was measured by flow cytometry. Ratios of median GFP and DsRed fluorescence from cells expressing DsRed-IRES-GFP NS were normalized to median GFP/DsRed ratios from cells expressing DsRed-IRES-GFP. Data was quantified from independent experiments (n = 3)

and is represented as mean ± SEM. Statistical analysis was performed using ordinary one-way ANOVA; E3 depletion only had a large and statistically significant effect on GFP NS stability in LKO cells ($P < 0.0001$).

(E) Parental and KO HeLa (top panel) and RPE1 (bottom panel) cells were treated with control or Pirh2 and KLHDC10 siRNA and transiently transfected with GFP NS and mCherry. Expression and gel mobility of GFP NS were analyzed by immunoblot. mCherry serves as a transfection control.

See also Figures S5 and S6.

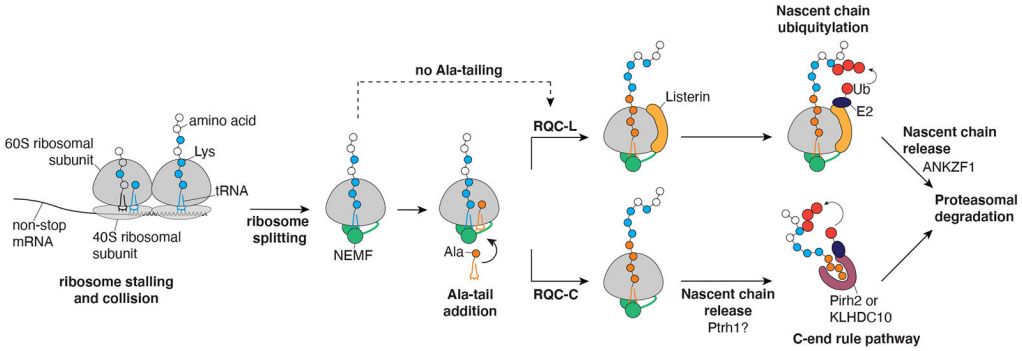

Figure 5. Model of the actions of Pirh2 and KLHDC10 in mammalian RQC

Exposure of 60S subunit-associated peptidyl-tRNA in response to ribosome stalling and splitting is the key trigger for NEMF recruitment, the first step in mammalian RQC. Subsequent ubiquitylation of the nascent-chain by Listerin promotes extraction and proteasomal degradation (RQC-L; L for Listerin). The extent to which NEMF elongates nascent-chains with Ala tails prior to Listerin-mediated ubiquitylation likely varies according to the Lys accessibility of each substrate, with the dashed arrow indicating situations in which C-terminal tailing is not required for Listerin to act. When Listerin action becomes limiting, NEMF-mediated Ala tails serve as a proteolytic signal for the E3 ligases Pirh2 and KLHDC10, which bind to and ubiquitylate the released nascent-chains (RQC-C; C for C-end rule pathway). Represented are: ribosomal subunits (grey), tRNA-Lys and Lys (blue), NEMF (green), tRNA-Ala and Ala (orange), Listerin (yellow), Ubiquitin (red), E2 (navy) and Pirh2 or KLHDC10 (magenta).

KEY RESOURCES TABLE

REAGENT or RESOURCE	SOURCE	IDENTIFIER
Antibodies		
Mouse monoclonal anti-GFP (clones 7.1 and 13.1)	Roche	Cat# 11814460001; RRID: AB_390913
Mouse monoclonal anti-FLAG M2	Sigma-Aldrich	Cat# F1804; RRID: AB_262044
Mouse monoclonal anti-HA	Biolegend	Cat# 901515; RRID: AB_2565334
Mouse monoclonal anti-mCherry (clone 1C51)	Abcam	Cat# ab125096; RRID: AB_11133266
Rabbit polyclonal anti-RFP	Thermo Fisher	Cat# R10367; RRID: AB_10563941
Mouse monoclonal anti-Tubulin (clone DM1A)	Sigma-Aldrich	Cat# T6199; RRID: AB_477583
Rabbit polyclonal anti-Listerin/RNF160	Abcam	Cat# ab104375; RRID: AB_10711159
Rabbit polyclonal anti-NEMF/SDCCAG1	Proteintech	Cat# 11840-1-AP; RRID: AB_2183413
Rabbit monoclonal anti-Pirh2/Rchy1	Abcam	Cat# ab189247
Goat polyclonal anti-GST	GE Healthcare	Cat# 27-4577; RRID: AB_771432
Mouse monoclonal anti-Ubiquitin (clone P4D1)	CST	Cat# 3936; RRID: AB_331292
Goat polyclonal anti-mouse IgG (H+L)-HRP	Dianova	Cat# 115-035-146; RRID: AB_2307392
Goat polyclonal anti-rabbit IgG (H+L)-HRP	Dianova	Cat# 111-035-144; RRID: AB_2307391
Rabbit polyclonal anti-goat IgG (H+L)-HRP	Dianova	Cat# 305-035-045; RRID: AB_2339403
Bacterial and Virus Strains		
BL21 (DE3)	E. Schiebel lab	NA
DH5α	E. Schiebel lab	NA
Chemicals, Peptides, and Recombinant Proteins		
G418	Roche	Cat# 04727894001
MG132 (Z-Leu-Leu-Leu-al)	Sigma-Aldrich	Cat# C2211-5MG
Bortezomib	Fisher Scientific	Cat# J60378.MB
MLN4924	Biomol	Cat# LKT-M4454
Lipofectamine 3000	Invitrogen	Cat# L3000015
Lipofectamine RNAiMax	Invitrogen	Cat# 13778150
Anti-FLAG® M2 magnetic beads	Sigma-Aldrich	Cat# A2220
GFP-Trap® magnetic agarose beads	Chromotek	Cat# gtma-20
GFP-Trap® agarose beads	Chromotek	Cat# gta-10
Protino Glutathione Agarose 4B	Machery-Nagel	Cat# 745500.10
Glutathione, reduced	Sigma-Aldrich	Cat# Y0000517

REAGENT or RESOURCE	SOURCE	IDENTIFIER
EDTA-free protease inhibitor	Roche	Cat# 04693159001
Ubiquitin (from bovine erythrocytes)	Sigma-Aldrich	Cat# U6253-5MG
UBA1 (mouse)	This study	NA
UBE2D2 (human)	D. Huang lab	NA
GST-Pirh2	This study	NA
GST-KLHDC10	This study	NA
GFP	This study	NA
GFP-Ala_6	This study	NA
GFP-Thr_6	This study	NA
Critical Commercial Assays		
RNeasy Mini Kit	Qiagen	Cat# 74104
QuantiTect Reverse Transcription Kit	Qiagen	Cat# 205311
LightCycler 480 SYBR Green I Master mix	Roche	Cat# 04707516001
DirectPCR Lysis Reagent	Viagen	Cat# 301-C
TOPO™ TA Cloning™	Invitrogen	Cat# 450030
ExpressPlus™ PAGE Gel, 4-20%	GenScript	Cat# M42010 Cat# M42012 Cat# M42015
NuPAGE™ 4-12%, Bis-Tris	Thermo Fisher	Cat# NP0321BOX
Color Prestained Protein Standard, Broad Range (11-245 kDa and 10-250 kDa)	New England Biolabs	Cat# P7712 Cat# P7719
Deposited Data		
PAR-CLIP	This study	PRJNA641646
Raw files of immunoblots	This study	http://dx.doi.org/10.17632/vytk5p9wn6.1
Experimental Models: Cell Lines		
HeLa NEMF KO	This work	N/A
HeLa LTN1 KO	This work	N/A
HeLa LTN1/NEMF KO	This work	N/A
RPE1	M. Kaulich lab	N/A
RPE1 LTN1 KO	This work	N/A
Flp-In™ T-REx™ 293 cells	Thermo Fisher	R78007
Oligonucleotides		
Silencer Select siRNA Negative Control No. 1	Invitrogen	Cat# 4390843
Silencer Select siRNA LTN1	Invitrogen	Cat# s25003
Silencer Select siRNA NEMF	Invitrogen	Cat# s17483
Silencer Select siRNA RCHY1/Pirh2	Invitrogen	Cat# s24703
Silencer Select siRNA KLHDC10	Invitrogen	Cat# s22820
Silencer Select siRNA KLHDC2	Invitrogen	Cat# s24149
Silencer Select siRNA KLHDC3	Invitrogen	Cat# s41938
Silencer Select siRNA UBE3C	Invitrogen	Cat# s18659

REAGENT or RESOURCE	SOURCE	IDENTIFIER
sgRNA sequences targeting *LTN1* (Exon 6) 5' CACCGATAAGGAACAAGTTACAACC 3' 3' CTATTCCTTGTTCAATGTTGGCAAA 5'	This paper	N/A
sgRNA sequences targeting *NEMF* (Exon 3) 5' CACCGCTAGACGGCATCATATTCTT 3' 3' CGATCTGCCGTAGTATAAGAACAAA 5'	This paper	N/A
Primers for PCR, see Table S3	This paper	N/A
Degron sequences for DsRed-IRES-GFP and pEGFP plasmids, see Table S4	This paper	N/A
Primers for qPCR, see Table S5	This paper	N/A
Recombinant DNA		
px458	Addgene; Feng Zhang	#48138
pENTR4	Thermo Fisher Scientific	#A10465
pENTR4 NEMF	This work	N/A
pFRT/TO/FLAG/HA-DEST	T. Tuschl lab	N/A
pFRT/TO/FLAG/HA-DEST NEMF WT	This work	N/A
pEGFP NS	This work	N/A
pEGFP-Ala_6	This work	N/A
pEGFP-Ala_4	This work	N/A
pEGFP-Thr_2-Ala_2	This work	N/A
pEGFP-Ala_5Leu	This work	N/A
pEGFP-Ala_5Phe	This work	N/A
pEGFP-Ala_5Val	This work	N/A
pEGFP NEMF-FLAG WT	This work	N/A
pEGFP NEMF-FLAG D96A R97A	This work	N/A
MSCV-CMV-DsRed-IRES-EGFP-DEST	Addgene; Stephen Elledge	#41941
pEGFP DsRed-IRES-GFP	This work	N/A
pEGFP DsRed-IRES-GFP NS	This work	N/A
pEGFP DsRed-IRES-GFP-Ala_1	This work	N/A
pEGFP DsRed-IRES-GFP-Ala_2	This work	N/A
pEGFP DsRed-IRES-GFP-Ala_3	This work	N/A
pEGFP DsRed-IRES-GFP-Ala_4	This work	N/A
pEGFP DsRed-IRES-GFP-Ala_5	This work	N/A
pEGFP DsRed-IRES-GFP-Ala_6	This work	N/A
pEGFP DsRed-IRES-GFP-Ala_5Thr	This work	N/A
pEGFP DsRed-IRES-GFP-Ala_4ThrAla	This work	N/A
pEGFP DsRed-IRES-GFP-Thr_2Ala_2	This work	N/A
pEGFP DsRed-IRES-GFP-Lys_4	This work	N/A
pEGFP DsRed-IRES-GFP-Lys_4Ala_4	This work	N/A
pEGFP DsRed-IRES-GFP-SelK	This work	N/A

REAGENT or RESOURCE	SOURCE	IDENTIFIER
pcDNA5 3xFLAG-Pirh2	This work	N/A
pcDNA5 3xFLAG-Pirh2 M176E	This work	N/A
pCMV3 KLHDC10	GenScript	HG26504-UT
pcDNA5 3xFLAG-KLHDC10	This work	N/A
pcDNA5 3xFLAG-KLHDC2	This work	N/A
pET15b GST-Pirh2	This work	N/A
pET15b GST-KLHDC10	This work	N/A
pETB28b Elongin B (a.a. 1-104)/Elongin C (a.a. 1-112)	This work	N/A
Software and Algorithms		
ImageJ	N/A	https://imagej.nih.gov/ij
FlowJo	FlowJo	https://www.flowjo.com
Prism8 for Mac OS X	Graphpad	https://www.graphpad.com
STAR-2.5.2a	Dobin et al., 2013	N/A
Cutadapt	http://journal.embnet.org/index.php/embnetjournal/article/view/200/458	https://cutadapt.readthedocs.io/en/v1.8.2/installation.html
R Studio Version 0.98.1060	Rstudio	https://www.rstudio.com/
PAR-CLIP suite	Garzia et al., 2017b	https://rnaworld.rockefeller.edu/PARCLIP_suite/